



The transition on North America from the warm humid Pliocene to the glaciated Quaternary traced by eolian dust deposition at a benchmark North Atlantic Ocean drill site

David Lang, Ian Bailey, Paul A. Wilson, Christopher J. Beer, Clara T. Bolton, Oliver Friedrich, Cherry Newsam, Megan R. Spencer, Marcus Gutjahr, Gavin L. Foster, et al.

► To cite this version:

David Lang, Ian Bailey, Paul A. Wilson, Christopher J. Beer, Clara T. Bolton, et al.. The transition on North America from the warm humid Pliocene to the glaciated Quaternary traced by eolian dust deposition at a benchmark North Atlantic Ocean drill site. *Quaternary Science Reviews*, 2014, 93, pp.125-141. 10.1016/j.quascirev.2014.04.005 . hal-01667989

HAL Id: hal-01667989

<https://hal.science/hal-01667989>

Submitted on 13 Apr 2018

HAL is a multi-disciplinary open access archive for the deposit and dissemination of scientific research documents, whether they are published or not. The documents may come from teaching and research institutions in France or abroad, or from public or private research centers.

L'archive ouverte pluridisciplinaire **HAL**, est destinée au dépôt et à la diffusion de documents scientifiques de niveau recherche, publiés ou non, émanant des établissements d'enseignement et de recherche français ou étrangers, des laboratoires publics ou privés.

North Atlantic Color Cycles

1 The transition on North America from the warm humid Pliocene to the 2 glaciated Quaternary traced by eolian dust deposition at a benchmark 3 North Atlantic Ocean drill site

4
5 David C. Lang¹, Ian Bailey^{1,2*}, Paul A. Wilson¹, Christopher J. Beer¹, Clara T.
6 Bolton^{1,3}, Oliver Friedrich^{1,4}, Cherry Newsam^{1,5}, Megan R. Spencer¹, Marcus
7 Gutjahr^{1,6}, Gavin L. Foster¹, Matthew J. Cooper¹, J. Andrew Milton¹

8 1. National Oceanography Centre Southampton, University of Southampton, Waterfront Campus,
9 European Way, Southampton SO14 3ZH, UK.

10 2. Present address: Camborne School of Mines, College of Engineering, Mathematics & Physical
11 Sciences, University of Exeter, Penryn Campus, Trelierve Road, Penryn, Cornwall TR10 9FE, UK.

12 3. Present address: Facultad de Geología, Universidad de Oviedo, Campus de Llamaquique, Jesús Arias
13 de Velasco s/n, 33005 Oviedo, Spain.

14 4. Present address: Institute of Earth Sciences, University of Heidelberg, Im Neuenheimer Feld 234-
15 236, 69120 Heidelberg, Germany

16 5. Present address: Earth Sciences, University College London, Gower Street, London WC1E 6BT,
17 UK.

18 6. Present address: GEOMAR Helmholtz Centre for Ocean Research Kiel, Wischhofstrasse 1-3, 24148
19 Kiel, Germany

20 *Corresponding author (email: I.Bailey@exeter.ac.uk)

21

22 Abstract

23 We present Plio-Pleistocene records of sediment color, %CaCO₃, foraminifer
24 fragmentation, benthic carbon isotopes ($\delta^{13}\text{C}$) and radiogenic isotopes (Sr, Nd, Pb) of
25 the terrigenous component from IODP Site U1313, a reoccupation of benchmark
26 subtropical North Atlantic Ocean DSDP Site 607. We show that (inter)glacial cycles
27 in sediment color and %CaCO₃ pre-date major northern hemisphere glaciation and are

North Atlantic Color Cycles

unambiguously and consistently correlated to benthic oxygen isotopes back to 3.3 million years ago (Ma) and intermittently so probably back to the Miocene/Pliocene boundary. We show these lithological cycles to be driven by enhanced glacial fluxes of terrigenous material (aeolian dust), not carbonate dissolution (the classic interpretation). Our radiogenic isotope data indicate a North American source for this dust (~3.3 to 2.4 Ma) in keeping with the interpreted source of terrestrial plant wax-derived biomarkers deposited at Site U1313. Yet our data indicate a mid latitude provenance regardless of (inter)glacial state, a finding that is inconsistent with the biomarker-inferred importance of glaciogenic mechanisms of dust production and transport. Moreover, we find that the relation between biomarker and the lithogenic component of dust accumulation is distinctly non-linear. Both records show a jump in glacial rates of accumulation from MIS G6 (2.72 Ma) onwards but the amplitude of this signal is about 3 to 8 times greater for biomarkers than for dust and particularly extreme during MIS 100 (2.52 Ma). We conclude that North America shifted abruptly to a distinctly more arid and windy glacial regime from MIS G6, but major shifts in glacial North American vegetation biomes and regional wind fields (exacerbated by the growth of a large Laurentide ice sheet during MIS 100) likely explain amplification of this signal in the biomarker records. Our findings are consistent with wetter-than-modern reconstructions of North American continental climate under the warm high CO₂ conditions of the Early Pliocene but contrast with most model predictions for the response of the hydrological cycle to anthropogenic warming over the coming 50 years (poleward expansion of the subtropical dry zones).

50

Keywords: Pliocene; Quaternary; eolian; dust; North America, North Atlantic; Laurentide Ice Sheet.

North Atlantic Color Cycles

53

54 **1. Introduction**

55 Deep-sea sediments in the climatically sensitive North Atlantic region are composed
56 of two main constituents: biogenic carbonate (CaCO_3) produced in the overlying
57 water column and allochthonous detrital material, with volcanic ash important only
58 locally. It has long been recognised that striking rhythmic changes in the abundance of
59 these constituents and therefore sediment color and % CaCO_3 (Figure 1) provide both
60 a high fidelity means of stratigraphic correlation and an expression of pronounced
61 climate variability, especially in sediments deposited during times of significant
62 northern hemisphere glaciation (NHG) (e.g. Ericson et al., 1961; Ruddiman and
63 Glover, 1972).

64 Shackleton et al. (1984) drew attention to the remarkable correspondence
65 between high amplitude changes in both benthic $\delta^{18}\text{O}$ and % CaCO_3 back to earliest
66 Pleistocene Marine Isotope Stage (MIS) 100 (2.52 Ma) at Deep Sea Drilling Project
67 (DSDP) Site 552, where sediment deposition is dominated by pelagic rain from
68 above. Prior to 2.52 Ma, variance in benthic $\delta^{18}\text{O}$ is unaccompanied by large
69 amplitude change in % CaCO_3 at Site 552 (Figure 1A). Originally, initiation of high-
70 amplitude variance in color and % CaCO_3 at this site was attributed by Shackleton et
71 al. (1984) to onset of major NHG with % CaCO_3 controlled by variations in the flux of
72 non-carbonate material transported by ice rafting. We now know that the exact timing
73 of the large decrease in % CaCO_3 in sediments deposited at Site 552 is obscured
74 because MIS G6 through 103 (2.72–2.58 Ma) fall in a core break (Raymo et al.,
75 1989). As it happens, however, extensive work elsewhere shows MIS 100 to be the
76 oldest glacial during which ice sheets were large enough (Ruddiman et al. 1987;
77 Maslin et al. 1998; Jansen and Sjöholm, 1991; Jansen et al. 2000; Kleiven et al. 2002;

North Atlantic Color Cycles

78 Bailey et al., 2013) and high latitude surface ocean temperatures cool enough
79 (Lawrence et al. 2009; 2010; Naafs et al. 2010) to initiate ice-rafting on a basin-wide
80 scale across the open North Atlantic Ocean.

81 In Figure 1A we show %CaCO₃ records from two further classic North
82 Atlantic drill sites, DSDP 607 and 609 located on the southern fringe and at the centre
83 of the last glacial IRD belt, respectively (Figure 2). Originally, %CaCO₃ variability at
84 these two sites prior to ~2.5 Ma was attributed to sea floor CaCO₃ dissolution, a
85 consequence of their greater water depth (Sites 609, ~3.9 km & 607, ~3.5 km, vs. 552
86 ~2.3 km, Figure 1A) and the influence of corrosive poorly ventilated southern-
87 sourced bottom waters (Ruddiman et al., 1987; Ruddiman and Raymo, 1988). Yet,
88 comparison of the %CaCO₃ plots compiled by Ruddiman et al. (1987) to records from
89 shallower more recently drilled sites (Figure 1A vs. 1B) reveals that the timing of the
90 initiation of marked lithological cycles in North Atlantic Ocean sediments is not a
91 simple function of water depth indicating the influence of some factor other than
92 CaCO₃ dissolution.

93 In principle, three mechanisms have the potential to deliver terrigenous
94 sediments to Site U1313. But negligible Pliocene rates of accumulation of sand-sized
95 IRD and volcanic grains at Integrated Ocean Drilling Program (IODP) Site U1313
96 (Bolton et al. 2010), the reoccupation of DSDP Site 607, confirms that the
97 contemporaneous variability seen in %CaCO₃ (Figure 1) is not a function of melting
98 icebergs over this classic site. Two alternative potential explanations must therefore be
99 considered: (1) Transport beyond the contemporary iceberg front by ocean currents of
100 fine-grained material delivered by ice-rafting to the Nordic Seas by the Greenland Ice
101 Sheet (Winkler, 1999; Jansen et al., 2000; Andrews 2000). (2) Transport of
102 continentally derived eolian dust from North Africa or from North America as inferred

North Atlantic Color Cycles

103 based on biomarker records (Naafs et al., 2012).

104 To better understand the control(s) on, and climatic significance of, %CaCO₃
105 variability of North Atlantic Ocean sediments deposited during the intensification of
106 northern hemisphere glaciation (iNHG) we present new orbital-resolution records of
107 carbonate dissolution, benthic $\delta^{13}\text{C}$, coarse lithic abundance and sediment %CaCO₃
108 for IODP Site U1313, and radiogenic isotopes datasets that track the provenance of
109 terrigenous inputs to this site. We show that lithological cycles in North Atlantic
110 sediments of Pliocene age are driven by enhanced glacial fluxes of terrigenous
111 material, not carbonate dissolution. Our provenance work indicates that the
112 terrigenous component at the site is dominated by eolian dust sourced from the mid
113 latitudes of North America – a result consistent with published interpretations of the
114 record from Site U1313 of biomarkers derived from higher plant leaf waxes (Naafs et
115 al., 2012). A sharp increase in the biomarker proxy for dust inputs to our study site
116 during MIS G6, 2.72 Ma, is interpreted to reflect the importance of glacial grinding
117 by a large North American ice sheet complex in amplifying dust inputs to the North
118 Atlantic Ocean during glacials from this time (Naafs et al., 2012). Comparison among
119 data sets, however, indicates strong non-linearity in coupling between the dust and
120 biomarker records indicating that a reappraisal is merited of the sequence of climatic
121 events that they record and the mechanisms involved.

122

123 **2. Materials & Methods**

124 *2.1. IODP Site U1313*

125 IODP Site U1313 is located at the base of the upper western flank of the Mid Atlantic
126 Ridge at a water depth of 3426 m, ~240 nautical miles northwest of the Azores
127 archipelago (41°N, 32.5°W), on the extreme southerly limit of the last glacial “IRD

North Atlantic Color Cycles

128 belt” (Ruddiman, 1977), a southwest-northeast trending band of maximum iceberg
129 melting and hence IRD deposition between ~40°N and 55°N in the Atlantic Ocean
130 (Figure 2). Site U1313 was drilled during IODP Expedition 306 and constitutes a
131 reoccupation of DSDP Site 607, a benchmark mid-depth site monitoring North
132 Atlantic Deep Water throughout the Plio-Pleistocene (Ruddiman et al., 1987; Raymo
133 et al., 1989; Ruddiman et al., 1989; Raymo et al., 1992; Raymo et al., 2004). Site
134 U1313 offers distinct advantages over its Site 607 precursor because it benefits from
135 recovery by modern coring methods and from application of a full suite of physical
136 property data collection and stratigraphic correlation techniques (Channel et al.,
137 2010).

138

139 *2.2. Stable isotope analysis, foraminifera fragmentation and chronology*

140 Samples from IODP Site U1313 were obtained at 10 cm resolution from 114.12 to
141 155.28 meters composite depth (mcd) and washed over a 63 µm sieve. The ratio
142 between fragments and whole foraminifera was established for the >150 µm fraction
143 where more than 300 whole foraminifera were present following Ivanova et al.
144 (2003). We focus our discussion on the interval 3.33 Ma (MIS MG1) to 2.41 Ma (MIS
145 95) covered by a published oxygen isotope stratigraphy (Bolton et al., 2010),
146 measured on the benthic foraminifera *Cibicidoides wuellerstorfi* (>212 µm). For
147 discussions of the younger Pleistocene portion of the Site U1313 record, we utilize the
148 age model of Naafs et al. (2012) based on benthic $\delta^{18}\text{O}$ datasets spanning three time
149 windows of the past 1 Myr (Stein et al., 2009; Feretti et al., 2010; Naafs et al., 2012)
150 and shipboard correlation (Expedition 306 Scientists, 2006) of sediment physical
151 properties (L^* , lightness) to the LR04 stack (Lisiecki and Raymo, 2005). We present a
152 new benthic $\delta^{13}\text{C}$ record from the samples analysed by Bolton et al. (2010) with an

North Atlantic Color Cycles

external analytical precision, based on replicate analysis of an in-house standard

calibrated to NBS-19, of $\pm 0.031\%$ (1σ).

2.3 Coarse lithic counts

The only high-resolution record of IRD deposition at Site U1313 for iNHG spans MIS

102-96 (Bolton et al., 2010). To improve our understanding of the history of IRD

deposition at our study site during MIS M2 (3.3 Ma) and between MIS G6 and MIS

102 (2.72–2.56 Ma), new coarse lithic counts were performed on the $>150\mu\text{m}$ size

fraction between, respectively, 152.98–154.98 mcd and 120.74–129.86 mcd. The

abundance of coarse lithics in Site U1313 sediments are very low throughout our

study interval and are extremely low in sediments deposited prior to MIS 100 (2.52

Ma). To generate a statistically significant record of sand IRD abundance in Site

U1313 sediments (expressed as IRD per gram of dry sediment) we therefore counted

all coarse IRD ($>150\mu\text{m}$) in each sample studied.

2.4. Sediment color

There is a long history of attempts to develop rapid-throughput proxy methods to

estimate sediment $\%\text{CaCO}_3$ from the spectral properties of sediments (e.g. Chester

and Elderfield, 1966). Use of optical lightness as an analytical tool in sediments

recovered by DSDP and IODP has its roots in late Quaternary studies (Balsam, 1981),

was pioneered by grey-scale analysis of photographs (e.g. Herbert and D'Hondt,

1990; Busch, 1991) and is now determined routinely from sediment color in

sediments of appropriate lithology. Sediment color can be defined using three

variables, a^* (red-green), b^* (blue-yellow) and L^* (lightness), that lie along mutually

perpendicular axes in color space. We obtained shipboard color reflectance data at 2

North Atlantic Color Cycles

178 cm resolution for Site U1313 from the IODP database website
179 (<http://iodp.tamu.edu/database/index.html>), generated using a modern version of the
180 split core automatic track reflectance spectrometer first trialled to remarkable effect
181 during Ocean Drilling Program (ODP) Leg 138 (Mix et al., 1992; Mix et al., 1995;
182 Ortiz et al., 1999). Here we employ records of L^* to represent sediment color.

183 A comparison of L^* data for Site U1313 and discrete %CaCO₃ measurements
184 generated post-cruise on sediments deposited during MIS 16–9 (640–320 ka; Stein et
185 al., 2009) illustrates that large variations in L^* for Site U1313 sediments deposited
186 over late Pleistocene glacial-interglacial cycles correspond to pronounced variations
187 (of ~30 %) in sediment %CaCO₃ (Figure 3). To improve our understanding of the
188 relationship between sediment color and %CaCO₃ for the Pliocene portion of the Site
189 U1313 record (for which L^* values are typically higher and amplitude change muted
190 relative to those documented for the Pleistocene) we generated 193 new %CaCO₃
191 estimates on small (~0.5 cc), discrete samples using a standard (LECO) combustion
192 technique following Stein et al. (2009).

193 To generate a high-resolution record of %CaCO₃ of Site U1313 sediments for
194 the past 3.3 Ma, we perform a least-squares linear regression between our new
195 discrete %CaCO₃ data (Figure 3C; n = 193), supplemented by the previously
196 published %CaCO₃ data (Figure 3B; n = 151 (Stein et al., 2009)), and 10 cm (5 point)
197 running average of the L^* data series (Figure 3D). The excellent linear correlation
198 ($r^2=+0.88$, $p<0.001$; Figure 3D) between these two variables indicates that our orbital-
199 resolution L^* -based estimates of %CaCO₃ are not strongly influenced by potential
200 complicating factors (e.g. changing composition of the non-CaCO₃ fraction (Balsam
201 et al., 1999)). This calibration is applicable to the task of generating a record of
202 %CaCO₃ for Site U1313 sediments of Pliocene through late Pleistocene age, but the

North Atlantic Color Cycles

203 resultant %CaCO₃ record can only be used to estimate eolian dust fluxes prior to the
204 late Pleistocene interval because of the error propagation associated with notable
205 delivery of IRD during late Pleistocene ice-rafting events, most notably the extreme
206 Heinrich events (see Section 3.3 (Stein et al., 2009; Naafs et al., 2013)). Fortunately,
207 our focus is on the origin and temporal evolution of terrigenous MARs at our study
208 site during the Pliocene where the linear fit is excellent and our new IRD record
209 demonstrates that the terrigenous sediment component contains negligible (i.e.
210 interglacial-like) ice-rafted sand-sized grains.

211

212 2.5. Radiogenic isotope data

213 The radiogenic isotope (Nd, Pb, Sr) composition of Atlantic Ocean sediment is well
214 established as a tracer of both eolian sediment (e.g. Grousset et al., 1998; Abouchami
215 and Zabel, 2003; Grousset and Biscaye, 2005) and ice rafted material (e.g. Revel et
216 al., 1996; Grousset et al., 2001; Fagel et al., 2002; Fagel et al., 2004; Fagel and
217 Matielli, 2011; Colville et al., 2011). These applications rely on regional differences in
218 circum-North Atlantic Ocean geology as a function of age and tectonic (metamorphic)
219 history.

220 To understand better the origin of the terrigenous component of Site U1313
221 Pliocene sediments, we have measured the Pb, Nd and Sr isotopic composition of
222 carbonate-free bulk terrigenous samples selected from peak glacials and interglacials
223 associated with the interval of iNHG (3.5–2.5 Ma; Mudelsee and Raymo (2005)).
224 Sample processing closely followed Gutjahr et al. (2007). Approximately 0.5 g of
225 crushed and homogenised bulk sediment was decarbonated using a Na acetate buffer,
226 and absorbed metals were removed with a 1M MgCl₂ solution. Authigenic coatings
227 were then removed using a 0.05 M hydroxylamine hydrochloride – 15 % acetic acid

North Atlantic Color Cycles

228 – 0.03 M Na–EDTA solution buffered to pH 4 with analytical grade NaOH in two
229 steps totalling 27 hours on a shaker table. Following removal of organic matter using
230 hydrogen peroxide and aqua regia, samples were pressure-dissolved in a HF-HNO₃
231 mixture.

232 Pure samples of Pb, Nd and Sr were extracted using standard procedures. The
233 Nd-isotope (¹⁴³Nd/¹⁴⁴Nd) and Pb-isotope ratios (²⁰⁶Pb/²⁰⁴Pb, ²⁰⁷Pb/²⁰⁴Pb and
234 ²⁰⁸Pb/²⁰⁴Pb) of our processed samples were measured at the University of
235 Southampton using a multi-collector inductively coupled plasma mass spectrometer
236 (MC-ICP-MS, Thermo Scientific Neptune). Neodymium isotopic compositions were
237 obtained using the method of Vance and Thirlwall (2002) through adjustment to a
238 ¹⁴⁶Nd/¹⁴⁴Nd value of 0.7219. Mass-bias corrected ratios were normalized to the given
239 ¹⁴³Nd/¹⁴⁴Nd value (0.512115) of the standard JNdi-1 (Tanaka et al., 2000). Mass bias
240 corrected Pb isotopic compositions were measured following a standard-sample
241 bracketing approach normalizing Pb isotopic compositions of NBS981 to the values
242 of Baker et al. (2004). The Strontium isotope composition (⁸⁷Sr/⁸⁶Sr) of these samples
243 was also measured at the University of Southampton using a thermal ionisation mass
244 spectrometer (ThermoFisher TRITON Plus). Total procedural blanks averaged 174pg,
245 106pg and 195pg for Nd, Sr and Pb, respectively. External precisions are calculated
246 (at 2 standard deviations) as the reproducibility of the following standards: JNdi-1
247 (Nd), NBS 987 (Sr) and NBS 982 (Pb). Precision is 0.000007 (<0.15 εNd), 0.000015,
248 0.047, 0.022 and 0.062 for ¹⁴³Nd/¹⁴⁴Nd, ⁸⁷Sr/⁸⁶Sr, ²⁰⁶Pb/²⁰⁴Pb, ²⁰⁷Pb/²⁰⁴Pb and
249 ²⁰⁸Pb/²⁰⁴Pb respectively. For convenience Nd isotope ratios are reported in epsilon
250 notation as:

$$\epsilon_{Nd} = \left[\frac{{}^{143}\text{Nd}/{}^{144}\text{Nd}_{\text{sample}}}{{}^{143}\text{Nd}/{}^{144}\text{Nd}_{\text{CHUR}}} - 1 \right] \times 10^4$$

251

North Atlantic Color Cycles

252

253 where $^{143}\text{Nd}/^{144}\text{Nd}_{\text{CHUR}}$ reflects the Chondrite Uniform Reservoir value of 0.512638
254 (Jacobsen and Wasserburg, 1980).

255 We assessed the provenance of terrigenous sediments deposited at Site U1313
256 by comparing their Pb, Sr and Nd isotopic compositions to equivalent radiogenic
257 isotopic compositions of potential source regions, which are based on our compilation
258 of discrete measurements made on circum-North Atlantic Ocean bedrock, terrestrial
259 loess outcrop, atmospheric aerosols, and continental ice and dust source-proximal
260 (core top and down-core) marine sediments and river samples (Figure 2a and 4 and
261 Supplementary Information). Potential source areas for IRD deposited in the North
262 Atlantic Ocean fall into three groups marked by a range of radiogenic isotope
263 compositions (Figure 2a and 4 (c.f. Thierens et al., 2012)). The old, primarily
264 Precambrian terranes of Greenland and North Eastern Canada (including the Labrador
265 Sea, Hudson Strait and Baffin Bay) comprise the “Canadian Province” (Dawes et al.,
266 2009). Paleocene to recent volcanic rocks found in Eastern Greenland, Iceland and the
267 Faeroe Islands comprise the “Volcanic Province”, local Azores volcanism may also
268 contribute material of this composition. Together, areas with their corresponding
269 compositions represent the high-latitude regions that constitute the most likely sites of
270 early ice sheet growth (e.g. Winkler et al., 1999; DeConto et al., 2008). Lower-latitude
271 ice rafting from Britain, Scandinavia or North America (the Appalachian terrane and
272 Grenville Province in the region of the Gulf of Saint Lawrence) were important
273 sources of ice-rafted material to the North Atlantic Ocean during the last glacial
274 maximum (Watkins et al., 2007). Owing to their similarities in Pb and Nd-Sr isotope
275 spaces, we group these three distinct geographic regions into a third province,
276 intermediate in age to the two high-latitude provinces. Eolian material sourced from

North Atlantic Color Cycles

the Sahara and North America has a similar geologic age and isotopic composition to the Fenoscandinavian tectonic terranes and the Gulf of St Lawrence region of North America, but is unequivocally distinct from high-latitude Volcanic Province material and Precambrian and Proterozoic Canadian and Greenland terranes in Nd-Sr space.

3. Results and Discussion

3.1. Stable isotope stratigraphy and sediment color

The record of benthic $\delta^{13}\text{C}$ at Site U1313 shows only modest glacial-interglacial variability with the exception of prominent excursions to low values during the large benthic $\delta^{18}\text{O}$ glacials MIS 100, 98 and 96 (Figure 5). This result is consistent with the record from predecessor Site 607 (Raymo et al., 1989), but the prominent (inter)glacial $\delta^{13}\text{C}$ signal established in MIS 100 is more pronounced in our record. Our record also resolves with higher fidelity earlier key glacials and illustrates, for example, that MIS M2 (~3.3 Ma), the first prominent excursion in benthic $\delta^{18}\text{O}$ to interrupt early Pliocene warmth, is not associated with a prominent benthic $\delta^{13}\text{C}$ excursion indicative of corrosive southern sourced waters.

Our L^* -derived record of sediment $\%\text{CaCO}_3$ at Site U1313 is shown in Figures 1A and 5 and reveals the expected North Atlantic pattern (lighter, CaCO_3 -rich sediments during interglacials and darker more terrigenous-rich intervals during glacials), but the fidelity of the signal and its unambiguous correlation to our benthic $\delta^{18}\text{O}$ series are remarkable back to 3.3 Ma (the base of our isotope record – Figure 5G). This relationship was postulated for Site U1313 based on shipboard correlation of L^* to the LR04 stack (Expedition 306 Scientists, 2006). Here we confirm, using our co-registered signal ($\%\text{CaCO}_3$ and benthic $\delta^{18}\text{O}$ determined from the same sediments) that variations in L^* at Site U1313 track changes in benthic $\delta^{18}\text{O}$ at this

North Atlantic Color Cycles

302 site across iNHG from 3.33 to 2.4 Ma. This result demonstrates that the onset of clear
303 glacial-interglacial lithological cycles at this site took place at least 800 kyr earlier
304 than the onset both of basin-wide ice rafting at MIS 100, 2.52 Ma, and of pronounced
305 glacial-interglacial variability in benthic $\delta^{13}\text{C}$ at our study site (Figure 5B).

306

307 *3.2. Abundance of the carbonate sedimentary component at Site U1313*

308 Pliocene sediments at Site U1313 are characterized by small variations in color and
309 %CaCO₃ relative to the higher amplitude changes that characterize the late
310 Pleistocene (Figure 1). High amplitude changes in Pleistocene %CaCO₃ (and color)
311 from the North Atlantic Ocean are often interpreted to reflect primarily changes in
312 carbonate production and dilution by other sediment components (e.g. Lototskaya et
313 al., 1998; Helmke and Bauch, 2001), while the lower amplitude %CaCO₃ variations
314 observed during the Pliocene at DSDP Sites 607 and 609 have been classically
315 attributed to dissolution on glacial-interglacial timescales (Ruddiman et al., 1987).
316 Our analysis, however, calls this classic interpretation into question. Calcareous
317 microfossils are extremely well preserved in Pliocene sediments from Site U1313
318 with foraminifera fragment counts typically well within the zero ΔCO_3 range of Le
319 and Shackleton (1992) (Figure 5A). The relationship between the fraction of CaCO₃
320 dissolved and that remaining is highly non-linear such that, when the CaCO₃ fraction
321 is large, substantial CaCO₃ must be dissolved to achieve small percentage variations
322 (Berger, 1971). For example, to generate a change in carbonate content of the order
323 observed at Site U1313/607 between about 3.3 and 2.8 Ma (~95% to 85%, Figure
324 5G), about 60% of the initial CaCO₃ must be dissolved. Such substantial dissolution
325 of CaCO₃ at Site U1313 is not consistent with the extremely well preserved
326 calcareous microfossils observed in these sediments. Thus, in contrast to the classic

North Atlantic Color Cycles

327 interpretation, CaCO_3 dissolution does not control carbonate content at Site
328 U1313/607 prior to MIS 100 and cannot be used to assess changes in North Atlantic
329 deep-water carbonate chemistry through time. Instead, the dominant controls must be
330 calcite production and/or terrigenous dilution (Ruddiman and McIntyre, 1976;
331 Ruddiman et al., 1987; Lototskaya et al., 1998; Helmke and Bauch, 2001).

332 A recently published record of alkenone accumulation from Site U1313 (Naafs
333 et al., 2010) reveals the onset of high amplitude glacial-interglacial changes in
334 alkenone accumulation, and therefore total export productivity (Bolton et al., 2010b;
335 Bolton et al., 2011), from ~2.72 Ma (MIS G6). The orbital signal in the alkenone data,
336 however, is of the wrong sign for carbonate productivity to control sediment color and
337 CaCO_3 burial (alkenone accumulation peaks during glacials whereas % CaCO_3 and
338 color, L^* , peak during interglacials; Figure 5C). Furthermore, our records demonstrate
339 that terrigenous accumulation peaks during glacials throughout our study interval and
340 not just from ~2.72 Ma onwards (Figure 5E). We conclude that the glacial-interglacial
341 signal in Pliocene sediment color and % CaCO_3 at Site U1313 is driven by addition of
342 terrigenous material. Next we assess the potential mechanisms by which this
343 terrigenous material might have been transported to our study site.

344

345 *3.3. Radiogenic isotopes and sediment provenance*

346 The Sr, Nd and Pb isotope composition of the bulk sediment terrigenous fraction
347 deposited at Site U1313 during peak interglacial and glacial conditions during iNHG
348 are shown in Figure 6. The Sr and Pb isotope composition of the samples analysed
349 display a relatively small range of variability, with $^{87}\text{Sr}/^{86}\text{Sr}$ ranging from 0.71664 to
350 0.72561 and $^{206}\text{Pb}/^{204}\text{Pb}$ ranging from 18.20 to 18.97 (Fig 7A and C, respectively).
351 Variation in ϵNd is more pronounced (ranging between -9.85 to -17.67), although

North Atlantic Color Cycles

352 most values fall between -13.9 and -16 (Figure 7B). Two samples (corresponding to
353 interglacials MIS G1 and 101) are indicative of volcanic material transported from
354 East Greenland or Iceland, or from the Azores volcanic islands. Remarkably, aside
355 from these two volcanically influenced exceptions, Nd, Sr and Pb isotope ratios show
356 no systematic difference between samples selected from peak glacial and peak
357 interglacial climate states (across a range in benthic $\delta^{18}\text{O} > 1.5\text{‰}$, Fig. 7D).

358 Based on the continuous presence of terrestrial leaf waxes in the Pliocene
359 sediments at our study site (a tracer of eolian dust in marine sediments at Site U1313;
360 Figure 5D), we know that at least some portion of the terrigenous fraction at Site
361 U1313 is composed of eolian dust. This biomarker record exhibits fluxes akin to those
362 observed for wind-blown leaf-waxes deposited in the Southern Ocean over the past ~4
363 Ma - where eolian dust is known to dominate the make-up of terrigenous sediments at
364 ODP Site 1090 (Martínez-García et al., 2011). Comparison of the Nd, Sr and Pb
365 isotope composition of Site U1313 terrigenous sediments to those of potential source
366 regions points to a definitive (non-volcanic) mid-latitude origin (Figures 6 and 7 and
367 Supplementary Information). This observation is paleoclimatically powerful because
368 it demonstrates that, prior to MIS G6 (>2.72 Ma), in a world characterized by only
369 incipient high latitude NHG (e.g. Bintanja and van de Wal, 2008), eolian dust supply
370 from the Sahara or North America is the only credible source capable of producing
371 orbital-scale cyclical variations in terrigenous inputs to our study site. Our data are
372 incompatible with a contribution from Greenland or Northern Canada, which are
373 widely inferred to have been the nucleation points of the earliest northern hemisphere
374 ice sheets (Winkler, 1999; Jansen et al., 2000; DeConto et al., 2008). In fact, where
375 present, sand-sized IRD and volcanic grains occur in only trace numbers (typically 0
376 to <0.1 grains/g) in sediments older than MIS G4 at Site U1313. This finding,

North Atlantic Color Cycles

377 together with the lack of a glacial-interglacial signal in our geochemical data, makes a
378 high-latitude or even an improbable mid-latitude glacial origin for the bulk
379 terrigenous fraction at Site U1313 untenable for sediments deposited prior to 2.7 Ma.
380 These findings indicate that the bulk terrigenous sediment component deposited at
381 Site U1313 between 3.3 Ma and 2.7 Ma is dominated by eolian dust.

382 We might expect a direct contribution from ice rafting to the terrigenous
383 sediment component at Site U1313 during glacials between ~2.72 Ma and 2.4 Ma
384 associated with the onset of significant NHG (Kleiven et al., 2002). As in the case of
385 the older part of our record, however, our grain counts reveal, accumulation rates of
386 sand-sized IRD in glacial sediments from MIS G4 onwards to be negligible (Figure
387 5). This result is in keeping with the location of Site U1313, situated far south
388 (~41°N) of the late Pliocene IRD belt (centred on ~53°N; Bailey et al., 2013) and on
389 only the southernmost fringe of the IRD belt even during the Last Glacial (Figure 1).
390 This finding, together with, the consistent mid-latitude geochemical provenance
391 indicated for terrigenous sediments deposited at Site U1313 leads us to conclude that,
392 throughout our Pliocene record, the contribution made by IRD deposition shed from
393 icebergs over site to the average radiogenic isotope composition of terrigenous
394 sediments is insignificant in comparison to the major player, eolian dust. Similarly,
395 despite evidence for abundant deposition of IRD in the higher latitude northeast North
396 Atlantic Ocean sourced from high-latitude Archaean and Proterozoic-aged terranes
397 during glacials since ~2.72 Ma (Bailey et al., 2013), the consistent mid-latitude
398 geochemical provenance that we report here for the terrigenous fraction at Site U1313
399 makes it extremely unlikely that transport of fine-grained IRD beyond the
400 contemporary iceberg front by ocean currents could be responsible for terrigenous
401 deposition at our study site from MIS G6 onwards.

North Atlantic Color Cycles

Similarities of the Nd and Sr isotopic composition of North American and Saharan eolian dust means that we must consider additional lines of evidence to pin down the source of the dust at Site U1313. Today, while most of the African-derived dust is driven westwards over the tropical North Atlantic by the Trade Winds, some dust is also transported northwards towards the North Atlantic, the Mediterranean and as far north as Northern Europe (Bergametti et al., 1989; Moulin et al., 1997; Kuss and Kremling, 1999; Kellog and Griffin, 2006). Three lines of evidence, however, support the notion that eolian dust deposition at our study site during iNHG is dominated by North American sources. First, spectral analysis of our record of terrigenous accumulation at Site U1313 reveals a dominant obliquity beat (with no strong precession signal) throughout our study interval that is in contrast to the pattern of variability in records of Saharan dust deposition (Fig. 8). Saharan dust deposition reveals the influence of obliquity from ~2.7 Ma, but precessional variability is important for at least the last 5 Ma (Tiedemann et al., 1994; DeMenocal, 2004)). Second, both modern wind trajectories (Figure 2B) and those modelled for both the last glacial maximum and Pliocene (Haywood et al., 2000; Hewitt et al., 2003; Pausata et al., 2011) indicate that Site U1313 is strongly influenced by intense westerly winds originating from the major present-day North American dust source region, the American Southwest (including all land between 125°W and 95°W and 25°N and 40°N) that incorporates the southwestern United States and parts of northern Mexico (Seager et al., 2007). Third, organic biomarker- and clay mineralogy-based provenance studies, respectively, independently link Pliocene Pleistocene eolian derived terrestrial high plant waxes at Site U1313 (Naafs et al., 2012) and Holocene eolian-derived material across the central North Atlantic (Grousset and Chesselet, 1986) to North American sources.

North Atlantic Color Cycles

427

428 *3.4. Records and mechanisms of North American eolian dust flux during Pliocene*

429 *iNHG*

430 Dust is both a signal and an agent of climate change (Martin et al., 1990; Kohfield and
431 Harrison, 2001; Mahowald et al., 2005; Winckler et al., 2008; Ganopolski et al., 2010;
432 Sun et al., 2010; McGee et al., 2010). To date, however, nearly all we know of the
433 history of eolian dust export from North America during Pliocene iNHG comes from
434 a single proxy biomarker record of terrestrial higher plant leaf wax (organic n-alkane)
435 deposition at Site U1313 (Naafs et al., 2012). That benchmark high-resolution record
436 shows that eolian-derived n-alkane and alkan-1-ols inputs to the North Atlantic Ocean
437 jumped to higher glacial values from ~2.7 Ma (MIS G6, Figure 5). Yet, these
438 biomarkers represent only a minor and often highly variable component of eolian dust
439 (Huang et al., 2000; Conte and Weber, 2003) so it is important to compare the proxy
440 biomarker record for dust deposition at Site U1313 with our record of variations in the
441 deposition of the terrigenous sediment component at this site.

442 Our record reveals that, while dust fluxes to our study site prior to the onset of
443 significant NHG at ~2.72 Ma are lower than those associated with Quaternary
444 glaciations, they are still high (up to 0.9 g/cm²/ka) and unambiguously mimic global
445 climate (as recorded by benthic $\delta^{18}\text{O}$) back to at least 3.3 Ma (Figure 5E). The two
446 published biomarker records reveal that, from ~2.7 Ma onwards, glacial accumulation
447 of the organic fraction of North American dust increases significantly during glacials
448 at Site U1313 (Figure 5D). We are careful not to interpret our terrigenous record as a
449 pure signal of lithogenic dust deposition from this time because our records show
450 evidence for a contribution from ice rafting during glacials from MIS G4 onwards
451 (albeit extremely small, see Section 3.3). But our record of the bulk terrigenous flux

North Atlantic Color Cycles

452 to Site U1313 places an upper limit on the potential magnitude of increase in eolian
453 dust flux to our study site that is possible during MIS G6 relative to background
454 interglacial values prior to this time: it can not be greater than a factor of about two
455 (Figure 5E). In fact, the peak fluxes that we record for the bulk terrigenous fraction
456 around 2.7 Ma ($\sim 2 \text{ g/cm}^2/\text{ka}$, Figure 5E) are similar to the lower end of the estimated
457 range of late Pleistocene glacial dust flux to the North Atlantic Ocean ($2\text{--}5 \text{ g/cm}^2/\text{ka}$;
458 Maher and Denis, 2001).

459 The jumps in glacial accumulation in both the biomarker records and our
460 terrigenous record from MIS G6 (2.72 Ma) onwards (Figures 5D and 5E) strongly
461 suggest that the North American continent shifted abruptly into a distinctly more
462 Pleistocene-like cold stage regime (cold, arid, and windy) from MIS G6. One
463 potential mechanism for the sudden jump in dust inputs to our study site from 2.72
464 Ma is the development of large ice-sheets on North America from MIS G6 onwards as
465 inferred by Naafs et al. (2012). Large ice sheets advancing over regolith-rich Pliocene
466 terrains (Clark and Pollard, 1998) provide an attractive mechanism for delivering fine-
467 grained sediments to mid-latitude outwash plains for eolian entrainment (Ganopolski
468 et al., 2010), but three lines of evidence call this interpretation into question. (1)
469 Typically, the biomarker component of atmospheric dust becomes wind-entrained
470 through ablation from living vegetation assisted by sand blasting (eolian abrasion)
471 rather than by the deflation of soils and glacial outwash plains in dust source regions
472 (Huang et al., 2000; Conte and Weber, 2002; Schefuß et al., 2003). (2) Recent work
473 on the provenance of North Atlantic IRD (Bailey et al. 2013) and on Arctic climate
474 (Bringham-Grette, 2013) during iNHG indicates that major ice sheets (i.e. extending
475 into the mid latitudes) are unlikely to have been sustained in North America as early
476 as during MIS G6. In fact, our data show that dust inputs to Site U1313 were likely

North Atlantic Color Cycles

substantial during cold stages well before MIS G6 with a particularly prominent peak in MIS M2 (Figure 5E), long before the existence of a large Laurentide ice sheet is tenable (De Schepper et al., 2013; Bringham-Grette et al., 2013). (3) Our radiogenic isotope data show a consistently mid-latitude provenance of the bulk terrigenous fraction at Site U1313 from 3.3 through 2.4 Ma regardless of glacial-interglacial state, thereby ruling out a significant high latitude contribution, even during MIS 100. These observations suggest that non-glaciogenic processes of Pliocene dust production, akin to those important during the last glacial maximum (e.g. increased wind intensity, enhanced aridity and reduced vegetation (Rea et al., 1994; Aleinikoff et al., 1999; Mason 2001; Werner et al., 2002; Bettis et al., 2003; Winkler et al., 2002; Prospero et al., 2002; Bussaca et al., 2003; Mahowald et al., 2006; Aleinikoff et al., 2008; McGee et al., 2010)), are more important than suggested previously.

3.5. Non-linearity in the relation between biomarkers and terrigenous eolian dust deposition in the North Atlantic Ocean during Pliocene intensification of northern hemisphere glaciation.

In Figure 9 we present cross plots of our record of terrigenous mass accumulation at Site U1313 and the published biomarker records of Naafs et al. (2012) for our study interval (3.33-2.41 Ma). These cross plots reveal a close association between biomarker and terrigenous sediment accumulation at our study site but, in contrast to what is seen in other paleo-dust proxy records (Winckler et al., 2008) including other applications of the n-alkane technique (e.g. at South Atlantic Site 1090; Figure 9C; Martinez-Garcia et al., 2011), the relationships observed between the biomarkers and terrigenous fraction in Site U1313 are distinctly non-linear (e.g. Figure 9A vs. 9B). While stratigraphic comparison of these three records shows that they all display

North Atlantic Color Cycles

502 jumps in glacial accumulation from MIS G6 (2.72 Ma) onwards (Section 3.4), the
503 amplitude of this signal is about 3 to 8 times greater for biomarkers than for
504 terrigenous inputs (Figure 10). The amplified jump in the biomarker records relative
505 to the jump in the terrigenous record is particularly extreme during MIS 100 (2.52
506 Ma), especially in the record of n-alkan-1-ol accumulation (Figure 10). This
507 observation underscores an important point: Non-linearity in the relation between the
508 biomarkers and the lithogenic record cannot be explained by invoking the input of
509 terrigenous material through additional mechanisms (ice rafting and volcanic inputs
510 are the only other viable mechanisms at Site U1313) because additional terrigenous
511 inputs would act to amplify our terrigenous record rather the biomarker record (ice
512 rafting control on biomarker flux is not documented even during the extreme Heinrich
513 events of the Late Pleistocene, Naafs et al. 2012). Furthermore, our records show that,
514 where present (low values from MIS G4), IRD accumulation rates are always higher
515 in glacials than in interglacials (sand-sized volcanic grains are extremely rare in Site
516 U1313 sediments throughout our study interval; Figure 5). Thus, there is no way to
517 explain amplification of the glacial jumps in the biomarker record (relative to the
518 terrigenous fraction) by invoking decreases in IRD and/or volcanics inputs while
519 a linear relation is maintained between biomarker and lithogenic dust. In other words,
520 our records point to the unequivocal existence of some mechanism that acts to
521 amplify the glacial jumps in the biomarker record relative to those in our terrigenous
522 record.

523 Amplification of the glacial biomarker signal from MIS G6, and particularly
524 during MIS 100 (Figure 10) points to increased efficiency of biomarker export/burial
525 (especially in n-alkan-1-ols) and/or major shifts in vegetation biomes relative to
526 preceding glacials. It seems an unlikely co-incidence that MIS 100 is the oldest glacial

North Atlantic Color Cycles

for which there exists convincing evidence from diverse proxy records for the existence of a major Laurentide Ice Sheet (Bailey et al., 2010; 2013; Bringham-Grette et al., 2013) extending well into the mid-latitudes (39° north based on the terrestrial record of glacial tills; Balco and Rovey, 2010). We hypothesize that some combination of a southward shift of boreal and temperate forest biomes across North America, strengthening of wind-driven sand-blasting and perhaps precipitation-led increase in woody plant cover (woody thickening) in arid regions south of the Laurentide Ice Sheet front may be responsible for the amplified glacial jumps in the biomarker records, especially the extreme signal seen in MIS 100. Our hypothesis requires testing but is consistent with the interpreted response of the atmosphere and vegetation to ice sheet advance well into the mid-latitudes during the Last Glacial Maximum (LGM) (e.g., Clark & Pollard, 1998; Kutzbach et al., 1998; Clark et al., 1999; Thompson and Anderson 2000; Huang et al., 2001; Prentice et al., 2011; Bragg et al., 2013; Ullman et al., 2014).

541

3.6. Eolian dust deposition in the North Atlantic Ocean during the warm Pliocene.

We argue that the onset of clear glacial-interglacial cycles in sediment color is driven by changes in terrigenous dust accumulation at Site U1313 and that these cycles appear at least 800 kyr earlier than MIS 100 and well before significant iNHG commenced around 2.72 Ma. In Figure 11 we assess how far back into the Pliocene Epoch these signals extend by comparing sediment color reflectance and estimated lithogenic dust flux from Site U1313 to published climate records for the entire Pliocene (to ~5.3 Ma, the base of LR04). The correspondence between sediment color at Site U1313 and global climate change registered by benthic $\delta^{18}\text{O}$ is remarkable. With the exception of one main interval of peak Pliocene warmth (4.3 to

North Atlantic Color Cycles

~4.0 Ma; Seki et al., 2012) when the sediment color reflectance record shows high values with little orbital structure and a minor contribution from lithogenic dust can be inferred, we observe the Pleistocene pattern (L^* minima during glacials; maxima during interglacials) at Site U1313 back to 5.3 Ma (the base of LR04, Fig. 11A).

In some respects, the signal of a minor lithogenic dust component during high CO_2 warm Pliocene conditions is expected because climate model simulations (e.g. Salzmann et al., 2008; 2013; Goldner et al., 2011) and paleo-data (e.g. Zarate and Fasana, 1989; Thompson, 1991; Smith, 1994; Axelrod, 1997; Salzmann et al., 2008, 2009, 2013; Jimenez-Moreno et al., 2010) for the warm Pliocene, particularly for the Mid-Piacenzian PRISM time-slab (Dowsett et al., 2012; Haywood et al., 2013), indicate noticeably wetter than modern conditions in modern arid and semi-arid regions, including the American Southwest. Yet in other respects our findings are surprising because there is broad consensus among climate model predictions for the future suggesting an increase in the expanse of arid to semi-arid mid-latitudes in a warmer world, and that this transition should already be underway in North America (e.g. Held and Soden, 2006; Seager et al., 2007; O’Gorman and Schneider, 2009).

Three main hypotheses have been suggested to explain the fundamental discrepancy between climate model predictions for the next 50 to 100 years and the model simulations of the warm Pliocene: (i) Differing boundary conditions, in particular the effect on regional precipitation fields of a potentially markedly lower elevation of the Pliocene Rocky Mountains (Wolf et al., 1997; Bonham et al., 2009) prior to the mid Pliocene (Foster et al., 2010). (ii) Enhanced regional precipitation in (southwest) North America relative to today in response to a warm eastern equatorial Pacific (Fig. 11B) in an El Niño-prone world (Goldner et al., 2011). (iii) Fundamental differences in the climate signal being modeled (equilibrium condition Pliocene

North Atlantic Color Cycles

577 climates incorporate both short and long-term feedbacks associated with climate
578 sensitivity while predictions for the non-equilibrium condition ‘climate transient’ of
579 the coming 50 years necessarily incorporate only fast or Charney feedbacks
580 (Salzmann et al., 2009)).

581 Each of these hypotheses makes different predictions for the timing of the
582 onset of source aridification and dust generation spatially through Pliocene time,
583 thereby presenting a means to test their validity. For example, the disappearance of
584 summer wet flora in North American terrestrial records that span the Miocene-
585 Pliocene boundary on both sides of the Cascades and Sierra Nevada mountains
586 suggests that aridification of the American West through the Mio-Pliocene is unlikely
587 to be related to a rain shadow effect due to mountain uplift (Lyle et al., 2008).
588 Similarly, based on global terrestrial vegetation reconstructions, the picture of a
589 wetter-than present warm Pliocene appears to be too extensive (Salzmann et al., 2009;
590 2013) to support the suggested role of North American mountain orography. But
591 while terrestrial records of precipitation balance provide powerful insights into
592 Pliocene climate (Salzmann et al., 2013), they are, by their nature, discontinuous in
593 coverage and often suffer from age control limitations. Plio-Pleistocene data coverage
594 for mid-latitude North America, including for the core of the present-day arid
595 American Southwest, is extremely poor because of the lack of lacustrine deposits
596 generally and Pleistocene glacial erosion in the north (Salzmann et al., 2009; 2013).
597 The secular signal in the Site U1313 record is broadly consistent with the
598 hypothesized importance of warm sea surface temperatures in the Pliocene eastern
599 equatorial Pacific (Fig. 11). Yet, many differences between early Pliocene and
600 present-day climates of parts of Africa, Asia, and Australia do not resemble the
601 anomalies associated with canonical El Niño teleconnections (Cane and Molnar,

North Atlantic Color Cycles

2007). Alongside model-based evaluation of the influence of fast versus slow feedbacks on precipitation balance and proxy reconstructions of the hydrological cycle, improved records of Pliocene dust deposition in well-dated marine sites recovered downwind from known Quaternary dust source regions will provide a valuable means to help understand the climatic response to sustained global warmth in the recent geological past.

4. Conclusions

We present Plio-Pleistocene records of sediment color, %CaCO₃, foraminifer fragmentation, benthic $\delta^{13}\text{C}$, coarse lithic counts and the radiogenic isotope (Nd, Sr, Pb) composition of terrigenous sediment component from IODP Site U1313. We demonstrate that glacial-interglacial cycles in sediment color are unambiguously correlated to benthic $\delta^{18}\text{O}$ back to at least 3.3 Ma, and represent changes in sediment %CaCO₃. Our new records of terrigenous and carbonate sediment accumulation rates, foraminifera fragmentation and benthic $\delta^{13}\text{C}$ show that these cycles are driven by enhanced glacial fluxes of terrigenous material and not glacial dissolution of carbonate material as previously interpreted.

On the basis of our radiogenic isotope data, we rule out a high-latitude origin for the terrigenous sediment component deposited at Site U1313 during our study interval and suggest that eolian dust sourced from mid latitude North America dominates clastic sediment deposition at this site during the Pliocene. This finding is consistent with previously published inferences on the provenance of an n-alkane biomarker proxy for dust inputs to our study site. Together with the biomarker records, our lithogenic data sets demonstrate that North America shifted abruptly to a distinctly more modern cold and arid glacial regime from MIS G6 with the

North Atlantic Color Cycles

627 development of a Laurentide ice sheet extending well into the mid-latitudes by MIS
628 100. Yet the relation between the biomarker and lithogenic component of dust
629 accumulation at Site U1313 is distinctly non-linear. Both records show a jump in
630 glacial rates of accumulation from ~2.7 Ma onwards (during MIS G6) but the
631 amplitude of this signal is about 3 to 8 times greater for biomarkers than for lithogenic
632 dust and particularly extreme during MIS 100 (2.52 Ma).

633 The development of significant continental ice in the northern hemisphere
634 during glacials from MIS G6 onwards undoubtedly had a profound impact on dust
635 generation on North America. Our analysis, however, suggests that glacial grinding
636 and transport of fine grained sediments to mid latitude outwash plains is not the
637 fundamental mechanism controlling the magnitude of the flux of higher plant leaf
638 waxes from North America to Site U1313 during iNHG. We hypothesize that some
639 combination of latitudinal biome shift, strengthening of sand-blasting south of North
640 American ice sheet front and perhaps precipitation-led woody thickening of arid
641 regions in response to ice sheet advance towards the mid-latitudes may be responsible
642 for the non-linearity observed. The secular pattern of change in the North Atlantic
643 record indicates that there existed a minor lithogenic dust component at our study site
644 during high-CO₂ peak Pliocene warm conditions (in contrast to climate model
645 predictions for the future suggesting an increase in the expanse of arid to semi-arid
646 zones in a warmer world). At least part of the discrepancy between climate model
647 predictions for enhanced aridity of the mid latitudes over next 50 to 100 years and
648 geologic observations for a warm wet Pliocene is likely attributable to fundamental
649 differences in the climate signal being observed for the Pliocene versus that being
650 modeled for future decades (equilibrium condition Pliocene climates versus transient
651 non-equilibrium model predictions for the future). The form of secular change shown,

North Atlantic Color Cycles

652 however, is broadly consistent with the hypothesized importance of warm sea surface
653 temperatures in the eastern equatorial Pacific during the Early Pliocene in bringing
654 about wetter-than-modern conditions in mid-latitude North America.

655

656 **5. Acknowledgements**

657 This research used samples provided by IODP, which was sponsored by the US
658 National Science Foundation and participating countries under management of Joint
659 Oceanographic Institutions, Inc. We thank the shipboard party of IODP Expedition
660 306. We also thank W. Hale and A. Wuelbers for help with sampling and D. Spanner,
661 M. Bolshaw and A. Michalik for laboratory assistance. We are grateful to the editor,
662 C. Hillaire-Marcel, two anonymous reviewers and Stijn de Schepper for detailed
663 constructive comments that helped to improve this manuscript. We thank Heiko
664 Pälike for his support and Ulrich Salzmann for discussions. I.B. is also grateful to UK
665 IODP for financial support for shipboard and post-cruise participation in IODP
666 Expedition 306. This study was supported by the Natural Environment Research
667 Council (NERC) in the form of a Ph.D studentship to D.C.L and a NERC UK IODP
668 grant NE/F00141X/1 to P.A.W and I.B. The data presented in this manuscript is
669 archived online at Pangaea ([doi.pangaea.de/10.101594/PANGAEA.829428](https://doi.org/10.101594/PANGAEA.829428)).

670

671 **6. References**

672 Abouchami, W., Zabel, M., 2003. Climate forcing of the Pb isotope record of
673 terrigenous input into the equatorial Atlantic. *Earth Planet. Sci. Lett.* 213, 221–
674 234.

675 Aleinikoff, J.N., Muhs, D.R., Sauer, R.R. & Fanning, C.M. 1999. Late Quaternary
676 loess in northeastern Colorado, II–Pb isotopic evidence for the variability of
677 loess sources. *Geological Society of America Bulletin* 111, 1876–1883.

North Atlantic Color Cycles

- 678 Aleinikoff, J.N., Muhs, D.R., Bettis, E.A., Johnson, W.C., Fanning, C.M., Benton, R.,
679 2008. Isotopic evidence for the diversity of late Quaternary loess in Nebraska:
680 Glaciogenic and nonglaciogenic sources. Geological Society of America
681 Bulletin 120 (11–12), 1362–1377.
- 682 Andrews, J.T., 2000. Icebergs and iceberg rafted detritus (IRD) in the North Atlantic:
683 Facts and Implications. Oceanogr. 13, 100–108.
- 684 Asmerom, Y., Jacobsen, S.B., 1993. The Pb isotopic evolution of the Earth:
685 inferences from river water suspended loads. Earth and Planetary Science
686 Letters 115, 245–256.
- 687 Axelrod, D.I., 1997. Outline history of California vegetation, in: Terrestrial
688 Vegetation of California, edited by: Barbour, M. and Major, J., New York,
689 John Wiley and Sons, 139–193.
- 690 Bailey, I., Bolton, C.T., DeConto, R.M., Pollard, D., Schiebel, R., Wilson, P.A., 2010.
691 A low threshold for North Atlantic ice rafting from “low-slung slippery” late
692 Pliocene ice sheets, Paleooceanography 25, PA1212,
693 doi:10.1029/2009PA001736.
- 694 Bailey, I., Foster, G.L., Wilson, P.A., Jovane, L., Storey, C.D., Trueman, C.N., J.
695 Becker, J., 2012. Flux and provenance of ice-rafted debris in the earliest
696 Pleistocene sub-polar North Atlantic Ocean comparable to the last glacial
697 maximum, Earth and Planetary Science Letters 341–344, 222–233,
698 doi:10.1016/j.epsl.2012.05.034.
- 699 Bailey, I., Hole, G.M., Foster, G.L., Wilson, P.A., Storey, C.D., Trueman, C.N.,
700 Raymo, M.E., 2013. An alternative suggestion for the Pliocene onset of major
701 northern hemisphere glaciation based the geochemical provenance of North
702 Atlantic Ocean ice-rafted debris, Quaternary Science Reviews 75, 181–194,

North Atlantic Color Cycles

- 703 doi:10.1016/j.quascirev.2013.06.004.
- 704 Baker, J., Peate, D., Waight, T., Meyzen, C., 2004. Pb isotopic analysis of standards
705 and samples using a 207Pb-204Pb double spike and thallium to correct for
706 mass bias with a double-focusing MC- ICP-MS. *Chemical Geology* 211, 275-
707 303, doi:10.1016/j.chemgeo.2004.06.030.
- 708 Balco G., Rovey C.W., II., 2010. Absolute chronology for major Pleistocene advances
709 of the Laurentide Ice Sheet. *Geology* 38, 795–798
- 710 Balsam, W.L., 1981. Late Quaternary sedimentation in the western North Atlantic:
711 Stratigraphy and paleoceanography. *Palaeogeog. Palaeoclimatol. Palaeoecol.*
712 35, 215–240.
- 713 Balsam, W.L., Deaton, B.C., Damuth, D.E., 1999. Evaluating optical lightness as a
714 proxy for carbonate in marine sediment cores. *Mar. Geol.* 161, 141–153.
- 715 Berger, W.H., 1971. Sedimentation of Planktonic Foraminifera. *Mar. Geol.* 11, 325-
716 358.
- 717 Bernstein, S., Kelemen, P.B., Tegner, C., Kurz, M.D., Blusztajn, J., Brooks, C.K.,
718 1998. Post-break up basaltic magmatism along the east Greenland tertiary
719 rifted margin. *Earth and Planetary Science Letters* 160, 845–862.
- 720 Biscaye, P.E., Grousset, F.E., Revel, M., Van der Gaast, S., Zielinski, G.A., Vaars, A.,
721 Kukla, G., 1997. Asian provenance of glacial dust (stage 2) in the Greenland
722 Ice Sheet Project 2 Ice Core. Summit, Greenland. *Journal of Geophysical*
723 Research 102, 26 76526 781.
- 724 Bergametti, G., Gomes, L., Coudegaussen, G., Rognon, P., Lecoustumer, M.N., 1989.
725 African Dust Observed over Canary Islands - Source-Regions Identification
726 and Transport Pattern for Some Summer Situations. *J. Geophys. Res.-Atmos.*
727 94, 14855–14864.

North Atlantic Color Cycles

- 728 Bettis, E.A., Muhs, D.R., Roberts, H.M., Wintle, A.G., 2003. Last Glacial loess in the
729 conterminous USA. *Quat. Sci. Revs.* 22, 1907–1946.
- 730 Bintanja, R., van de Wal, R.S.W., 2008. North American ice-sheet dynamics and the
731 onset of 100,000-year glacial cycles. *Nature* 454, 869–872,
732 doi:1038/nature07158.
- 733 Bolton, C.T., Wilson, P.A., Bailey, I., Friedrich, O., Beer, C.J., Becker, J., Baranwal,
734 S., Schiebel, R., 2010a. Millennial-scale climate variability in the subpolar
735 North Atlantic Ocean during the late Pliocene. *Paleoceanog.* 25, PA4218,
736 doi:10.1029/2010PA001951.
- 737 Bolton, C.T., Lawrence, K.T., Gibbs, S.J., Wilson, P.A., Cleaveland, L.C., Herbert,
738 T.D., 2010b, Glacial–interglacial productivity changes recorded by alkenones
739 and microfossils in late Pliocene eastern equatorial Pacific and Atlantic
740 upwelling zones. *EPSL* 295, 401–411.
- 741 Bolton, C.T., Lawrence, K.T., Gibbs, S.J., Wilson, P.A., Herbert, T.D., 2011. Biotic
742 and geochemical evidence for a global latitudinal shift in ocean
743 biogeochemistry and export productivity during the late Pliocene. *EPSL* 308,
744 (1–2), 200–210, <http://dx.doi.org/10.1016/j.epsl.2011.05.046>.
- 745 Bonham, S.G., Haywood, A.M., Lunt, D.J., Collins, M., Salzmann, U., 2009. El
746 Niño–Southern Oscillation, Pliocene climate and equifinality. *Phil. Trans. R.*
747 *Soc. A* (2009) 367, 127–156, doi:10.1098/rsta.2008.0212
- 748 Brigham-Grette, J. et al., 2013. Pliocene Warmth, Polar Amplification, and
749 Stepped Pleistocene Cooling Recorded in NE Arctic Russia. *Science*
750 340(6139), 1421–1427, doi:10.1126/science.1233137.
- 751 Bragg, F.J., Prentice, I.C., Harrison, S.P., Eglinton, G., Foster, P.N., Rommerskirchen,
752 F., Rullkötter, J., 2013. Stable isotope and modelling evidence for CO₂ as a

North Atlantic Color Cycles

- 753 driver of glacial--interglacial vegetation shifts in southern Africa.
754 Biogeosciences 10(3), 2001–2010, www.biogeosciences.net/10/2001/2013/
755 doi:10.5194/bg-10-2001-2013.
- 756 Busacca, A.J., Beget, J.E., Markewich, H.W., Muhs, D.R., Lancaster, N., Sweeney,
757 M.R., 2004. Eolian sediments. In: Gillespie, A.R., Porter, S.C., Atwater, B.R.
758 (Eds.), *The Quaternary Period in the United States*. Elsevier, Amsterdam, The
759 Netherlands, pp. 275–310.
- 760 Busch, W.H., 1991. Analysis of wet-bulk density and sediment color cycles in
761 Pliocene-Pleistocene sediments of the Owen Ridge (Site 722) and Oman
762 Margin (Site 728). In: Prell, W.L., Niitsuma, N., et al., *Proc. ODP, Sci. Results*,
763 117: College Station, TX (Ocean Drilling Program), 239–253.
- 764 Channell, J.E.T., Sato, T., Kanamatsu, T., Stein, R., Alvarez Zarikian C., 2010.
765 Expedition 303/306 synthesis: North Atlantic climate, *Proceedings of the*
766 *Integrated Ocean Drilling Program 303/306*,
767 doi:10.2204/iodp.proc.303306.214.
- 768 Chester, R., Elderfield, H., 1966. The infra-red determination of total carbonate in
769 marine carbonate sediments. *Chem. Geol.* 1, 277–290.
- 770 Clark, P.U., Pollard, D., 1998. Origin of the Middle Pleistocene Transition by ice
771 sheet erosion of regolith. *Paleoceanography* 13(1), 1–9,
772 doi:10.1029/97PA02660.
- 773 Clark, P. U., Alley, R.B., Pollard, D., 1999. Northern Hemisphere Ice-Sheet Influences
774 on Global Climate Change. *Science* 286, 1104–1111,
775 doi:10.1126/science.286.5442.1104
- 776 Cohen, R.S., O’Nions, R.K., 1982. The lead, neodymium and strontium isotopic
777 structure of ocean ridge basalts. *Journal of Petrology* 23, 299–324.

North Atlantic Color Cycles

- 778 Cole, J.M., Goldstein, S.L., deMenocal, P.B., Hemming, S.R., Grousset, F.E., 2009.
779 Contrasting compositions of Saharan dust in the eastern Atlantic Ocean during
780 the last deglaciation and African Humid Period. *Earth and Planetary Science*
781 *Letters* 278, 257–266.
- 782 Colville, E.J., Carlson, A.E., Beard, B.L., Hatfield, R.G., Stoner, J.S., Reyes, A.V.,
783 Ullman, D.J., 2011. Sr-Nd-Pb isotope evidence for ice-sheet presence on
784 Southern Greenland during the last interglacial. *Science* 333, 620–623.
- 785 Conte, M.H., Weber, J.C., 2002. Long-range atmospheric transport of terrestrial
786 biomarkers to the western North Atlantic. *Global Biogeochem. Cycles* 16 (4),
787 1142, doi:10.1029/2002gb001922.
- 788 Conte, M.H., Weber, J.C., Carlson, P.J., Flanagan, L.B., 2003. Molecular and carbon
789 isotopic composition of leaf wax in vegetation and aerosols in a northern
790 prairie ecosystem. *Oecologia* 135 (1), 67–77, doi:10.1007/s00442-002-1157-4.
- 791 Dawes, P.R. 2009. The bedrock geology under the Inland Ice: the next major
792 challenge for Greenland mapping *Geol. Surv. Denmark Greenland Bull.* 17,
793 57.
- 794 DeConto, R.M., Pollard, D., Wilson, P.A., Palike, H., Lear, C.H., Pagani, M., 2008.
795 Thresholds for Cenozoic bipolar glaciation. *Nature* 455, 652–656.
- 796 DeMenocal, P.B., 2004. African climate change and faunal evolution during the
797 Pliocene-Pleistocene. *EPSL* 220, 3–24.
- 798 De Schepper, S., Groeneveld, J., Naafs, B.D.A., Van Renterghem, C., Hennissen, J.,
799 Head, M.J., Louwye, S., Fabian, K., 2013. Northern Hemisphere Glaciation
800 during the Globally Warm Early Late Pliocene. *PLoS ONE* 8(12), e81508,
801 doi:10.1371/journal.pone.0081508
- 802 Dowsett, H.J. et al., 2012. Assessing confidence in Pliocene sea surface temperatures

North Atlantic Color Cycles

- 803 to evaluate predictive models. *Nature Clim. Change* 2, 365–371, doi:
804 10.1038/NCLIMATE1455.
- 805 Ericson, D.B., Ewing, M., Wollin, G., Heezen, B.C., 1961. Atlantic deep-sea sediment
806 cores. *Geol. Soc. Am. Bull.* 72, 193–286.
- 807 Expedition 306 Scientists, 2006. Site 1313, in *North Atlantic Climate, Proc. Integr.*
808 *Ocean Drill. Program*, 303/306, doi:10.2204/iodp.proc.303306.112.2006.
- 809 Fagel, N., Innocent, C., Gariépy, C., Hillaire-Marcel, C., 2002. Sources of Labrador
810 Sea sediments since the Last Glacial Maximum inferred from Nd-Pb isotopes,
811 *Geochim. Cosmochim. Acta* 66, 2569–2581.
- 812 Fagel N., Hillaire-Marcel, C., Humblet, M., Brasseur, R., Weis, D., Stevenson, R.,
813 2004. Nd and Pb isotope signatures of the clay-size fraction of Labrador Sea
814 sediments during the Holocene: Implications for the inception of the modern
815 deep circulation pattern. *Paleoceanography* 19, PA3002, doi
816 10.1029/2003PA000993.
- 817 Fagel, N., Mattielli, N., 2011. Holocene evolution of deep circulation in the northern
818 North Atlantic traced by Sm, Nd and Pb isotopes and bulk sediment
819 mineralogy, *Paleoceanography* 26, PA4220, doi:10.1029/2011PA002168.
- 820 Farmer, G.L., Barber, D., Andrews, J., 2003. Provenance of late Quaternary ice-
821 proximal sediments in the North Atlantic: Nd, Sr and Pb isotopic evidence.
822 *Earth and Planetary Science Letters* 209, 227–243.
- 823 Ferretti, P., Crowhurst, S.J., Hall, M.A., Cacho, I., 2010. North Atlantic millennial-
824 scale climate variability 910 to 790 ka and the role of the equatorial insolation
825 forcing. *Earth Planet. Sci. Lett.* 293, 24–41. doi:10.1016/j.epsl.2010.02.016.
- 826 Ford, H.L., Ravelo, A.C., Hovan, S., 2012. A deep Eastern Equatorial Pacific
827 thermocline during the early Pliocene warm period, *Earth and Planetary*

North Atlantic Color Cycles

- 828 Science Letters 355–356, 151–161,
829 <http://dx.doi.org/10.1016/j.epsl.2012.08.027>
- 830 Foster, G.L., Lunt, D.J., Parrish, R.R., 2010. Mountain uplift and the glaciation of
831 North America—a sensitivity study. *Climate of the Past* 6(5), 707–717.
- 832 Ganopolski, A., Calov, R., Claussen, M., 2010. Simulation of the last glacial cycle
833 with a coupled climate ice-sheet model of intermediate complexity. *Clim. Past*
834 6 (2), 229–244. doi:10.5194/cp-6-229-2010.
- 835 Gillette, D., 1999. A qualitative geophysical explanation for “hot spot” dust source
836 regions. *Contrib. Atmos. Phys.* 72, 67–77.
- 837 Goldner, A., Huber, M., Diffenbaugh, N., Caballero, R. 2011. Implications of the
838 permanent El Niño teleconnection “blueprint” for past global and North
839 American hydroclimatology. *Clim. Past*, 7, 723–743, 2011 □ [www.clim-](http://www.clim-past.net/7/723/2011/)
840 [past.net/7/723/2011/](http://www.clim-past.net/7/723/2011/) □ doi:10.5194/cp-7-723-2011.
- 841 Goldstein, S.J., Jacobsen, S.B., 1988. Nd and Sr isotopic systematics of river water
842 suspended material: implications for crustal evolution. *Earth and Planetary*
843 *Science Letters* 87, 249–265, [http://dx.doi.org/10.1016/0012-821X\(88\)90013-](http://dx.doi.org/10.1016/0012-821X(88)90013-1)
844 1.
- 845 Grousset, F.E., Chesselet, R., 1986. The Holocene sedimentary regime in the northern
846 Mid-Atlantic Ridge region. *Earth Planet. Sci. Lett.* 78, 271–287.
- 847 Grousset, F.E., Parra, M., Bory, A., Martinez, P., Bertrand, P., Shimmield, G., Ellam,
848 R.M., 1998. Saharan wind regimes traced by the Sr–Nd isotopic composition
849 of subtropical Atlantic sediments: Last Glacial Maximum vs today. *Quat. Sci.*
850 *Rev.* 17, 395–409, [http://dx.doi.org/10.1016/S0277-3791\(97\)00048-6](http://dx.doi.org/10.1016/S0277-3791(97)00048-6).
- 851 Grousset, F.E., Cortijo, E., Huon, S., Hervé, L., Richter, T., Burdloff, D., Duprat, J.,
852 Weber, O., 2001. Zooming in on Heinrich layers. *Paleoceanography* 16, 240–

North Atlantic Color Cycles

- 853 259, doi:10.1029/2000PA000559.
- 854 Grousset, F.E., Biscaye, P.E. 2005. Tracing dust sources and transport patterns using
855 Sr, Nd and Pb isotopes. *Chem. Geol.* 222, 149–167.
- 856 Gutjahr, M., Frank, M., Stirling, C.H., Klemm, V., van der Flierdt, T., Halliday, A.N.
857 2007. Reliable extraction of a deepwater trace metal isotope signal from Fe-
858 Mn oxyhydroxide coatings of marine sediments. *Chem. Geol.* 242, 351–370.
- 859 Hansen, H., Nielsen, T.F.D., 1999. Crustal contamination in Palaeogene east
860 Greenland flood basalts: plumbing system evolution during continental rifting.
861 *Chemical Geology* 157, 89–118, [http://dx.doi.org/10.1016/S0009-](http://dx.doi.org/10.1016/S0009-2541(98)00196-X)
862 2541(98)00196-X.
- 863 Haywood, A.M., Sellwood, B.W., Valdes, P.J., 2000. Regional warming: Pliocene (3
864 Ma) paleoclimate of Europe and the Mediterranean. *Geology* 28, 1063–1066
- 865 Haywood, A.M., Dolan, A.M., Pickering, S.J., Dowsett, H.J., McClymont, E.L.,
866 Prescott, C.L., Salzmann, U., Daniel J. Hill, D.J., Stephen J. Hunter, S.J.,
867 Daniel J. Lunt, D.J., Pope, J.O., Valdes P.J., 2013. On the identification of a
868 Pliocene time slice for data–model comparison. *Phil. Trans. R. Soc. A.* 371,
869 20120515, doi:10.1098/rsta.2012.0515
- 870 Held, I.M., Soden, B.J., 2006. Robust responses of the hydrological cycle to global
871 warming. *J. Climate* 19, 5686–5699, doi:10.1175/JCLI3990.1.
- 872 Helmke, J., Bauch, H., 2001. Glacial-interglacial relationship between carbonate
873 components and sediment reflectance in the North Atlantic. *Geo-Marine*
874 *Letters* 21, 16–22, doi:10.1007/s003670100067.
- 875 Herbert, T.D., D'Hondt, S., 1990. Precessional climate cyclicity in Late Cretaceous–
876 early Tertiary marine sediments: a high resolution chronometer of Cretaceous–
877 Tertiary boundary events. *EPSL* 99, 263–275.

North Atlantic Color Cycles

- 878 Hewitt, C.D., Stouffer, R.A., Broccoli, A.J., Mitchell, J.F.B, Valdes, P.J., 2003. The
879 effect of ocean dynamics in a coupled GCM simulation of the Last Glacial
880 Maximum. *Clim. Dyn.* 20 (2), 203–218.
- 881 Huang, Y.S., Dupont, L., Sarinthein, M., Hayes, J.M., Eglinton, G., 2000. Mapping of
882 C4 plant input from North West Africa into North East Atlantic sediments.
883 *Geochimica et Cosmochimica Acta* 64, 3505–3513.
- 884 Huang, Y.A., Street-Perrott, F.A., Metcalfe, S.E., Brenner, M., Moreland, M.,
885 Freeman, K.H., 2001. Climate change as the dominant control on glacial-
886 interglacial variations in C3 and C4 plant abundance. *Science* 293(5535),
887 1647–1651, doi:10.1126/science.1060143.
- 888 Ivanova, E., Schiebel, R., Singh, A.D., Schmiedl, G., Niebler, H.S, Hemleben, C.,
889 2003. Primary production in the Arabian Sea during the last 135000 years,
890 *Palaeogeogr. Palaeoclimatol. Palaeoecol.* 197, 61–82, doi:10.1016/S0031-
891 0182(03)00386-9.
- 892 Jacobsen, S.B., Wasserburg, G.J., 1980. Sm–Nd isotopic evolution of chondrites.
893 *Earth and Planetary Science Letters* 50 (1), 139–155.
- 894 Jansen, E., Sjöholm, J., 1991. Reconstruction of glaciation over the past 6 Myr from
895 ice-borne deposits in the Norwegian Sea. *Nature* 349, 600–603.
- 896 Jansen, E., Fronval, T., Rack, F., Channell, J.E.T., 2000. Pliocene-Pleistocene Ice
897 Rafting History and Cyclicity in the Nordic Seas During the Last 3.5 Myr.
898 *Paleoceanog.* 15, 709–721.
- 899 Jimenez-Moreno, G., Fauquette, S., and Suc, J. P., 2010. Miocene to Pliocene
900 vegetation reconstruction and climate estimates in the Iberian Peninsula from
901 pollen data. *Review of Palaeobotany and Palynology* 162, 403–415.
- 902 Juteau, M., Michard, A., Albarede, F., 1986. The Pb–Sr–Nd isotope geochemistry of

North Atlantic Color Cycles

- 903 some recent circum-Mediterranean granites. *Contributions to Mineralogy and*
904 *Petrology* 92, 331–340.
- 905 Kalnay, E., and Coauthors, 1996. The NCEP/NCAR 40-year Reanalysis Project. *Bull.*
906 *Amer. Meteor. Soc.* 77, 437–472.
- 907 Kellogg, C.A., Griffin, D.W., 2006. Aerobiology and the global transport of desert
908 dust. *Trends in Ecology and Evolution* 21(11), 638–644.
- 909 Kleiven-F, H., Jansen, E., Fronval, T., Smith, T.M., 2002. Intensification of Northern
910 hemisphere glaciations in the circum Atlantic region (3.5-2.4 Ma) -ice-rafted
911 detritus evidence. *Palaeogeogr., Palaeoclimatol., Palaeoecol.*, 184, 213–223.
- 912 Kohfeld, K.E., Harrison, S.P., 2001. DIRTMAP: The geological record of dust. *Earth*
913 *Science Reviews* 54: 81–114, [http://dx.doi.org/10.1016/S0012-](http://dx.doi.org/10.1016/S0012-8252(01)00042-3)
914 8252(01)00042-3.
- 915 Kokfelt T. F., Hoernle K. A. J., Hau□, F., Fiebig J., Werner R., Garbe-Schonberg D.,
916 2006. Combined trace element and Pb–Nd–Sr–O isotope evidence for recycled
917 oceanic crust (upper and lower) in the Iceland mantle plume. *Journal of*
918 *Petrology* 47, 1705–1749.
- 919 Kuss, J., Kremling, K., 1999. Particulate trace element fluxes in the deep northeast
920 Atlantic Ocean. *Deep-Sea Research Part I-Oceanographic Research Papers* 46,
921 149–169, [http://dx.doi.org/10.1016/S0967-0637\(98\)00059-4](http://dx.doi.org/10.1016/S0967-0637(98)00059-4).
- 922 Kutzbach, J.E., Gallimore, R., Harrison, S.P., Behling, P., Selin, R., Laarif, F., 1998.
923 Climate and biome simulations for the past 21,000 years, *Quaternary Science*
924 *Reviews* 17, 473–506, [http://dx.doi.org/10.1016/S0277-3791\(98\)00009-2](http://dx.doi.org/10.1016/S0277-3791(98)00009-2)
- 925 Lawrence, K.T., Liu, Z.H., Herbert, T.D., 2006. Evolution of the eastern tropical
926 Pacific through Plio-Pleistocene glaciation. *Science* 312, 79–83.
- 927 Lawrence, K.T., Herbert, T.D., Brown, C.M., Raymo, M.E., Haywood, A.M., 2009.

North Atlantic Color Cycles

- 928 High-amplitude variations in North Atlantic sea surface temperature during the
929 early Pliocene warm period. *Paleoceanog.* 24, PA2218,
930 doi:10.1029/2008PA001669.
- 931 Lawrence, K.T., Sosdian, S., White, H.E., Rosenthal, Y., 2010. North Atlantic climate
932 evolution through the Plio-Pleistocene climate transitions. *EPSL* 300, 329-342.
- 933 Le, J., Shackleton, N.J., 1992. Carbonate dissolution fluctuations in the Western
934 Equatorial Pacific during the late Quaternary. *Paleoceanog.* 7, 21-42.
- 935 Lisiecki, L.E., Raymo, M.E., 2005, A Pliocene-Pleistocene stack of 57 globally
936 distributed benthic $\delta^{18}\text{O}$ records. *Paleoceanog.* 20, PA1003,
937 doi:10.1029/2004PA001071.
- 938 Lototskaya, A., Ziveri, P., Ganssen, G.M., van Hinte, J.E., 1998. Calcareous
939 nannofloral response to Termination II at 45°N, 25°W (northeast Atlantic).
940 *Mar. Micropal.* 34, 47-70.
- 941 Lunt, D.J., Foster, G.L., Haywood, A.M., Stone, E., 2008. Late Pliocene Greenland
942 glaciation controlled by a decline in atmospheric CO₂ levels. *Nature* 454,
943 1102-1105.
- 944 Lyle, M., Barron, J., Bralower, T.J., Huber, M., Olivarez Lyle, A., Ravelo, A.C., Rea,
945 D.K., P.A. Wilson, P.A., 2008. Pacific Ocean and Cenozoic evolution of
946 climate. *Rev. Geophys.* 46, RG2002, doi:10.1029/2005RG000190.
- 947 Maher, B.A., Dennis, P.F., 2001. Evidence against dust mediated control of glacial-
948 interglacial changes in atmospheric CO₂. *Nature* 411, 176-180.
- 949 Mahowald, N.M., Baker, A.R., Bergametti, G., Brooks, N., Duce, R.A., Jickells, T.D.,
950 Kubilay, N., Prospero, J.M., Tegen, I., 2005. Atmospheric global dust cycle
951 and iron inputs to the ocean. *Global Biogeochemical Cycles* 19 (4), B4025,
952 doi:10.1029/2004GB002402.

North Atlantic Color Cycles

- 953 Mahowald, N.M., Yoshioka, M., Collins, W. Conley, A., Fillmore, D., Coleman, D. ,
954 2006. Climate response and radiative forcing from mineral aerosols during the
955 glacial maximum, pre-industrial, current and doubled-carbon dioxide climates,
956 GRL 33, L20705, doi:10.1029/2006GL026126.
- 957 Martin, J.H., 1990. Glacial-interglacial CO₂ change: The iron hypothesis,
958 Paleocanog. 5(1), 1–13, doi:10.1029/PA005i001p00001.
- 959 Martínez-García, A., Rosell-Melé, A., Jaccard, S.L., Geibert, W., Sigman, D.M., et al.,
960 2011. Southern Ocean dust–climate coupling over the past four million years.
961 Nature 476, 312–315, doi:10.1038/nature10310.
- 962 Maslin, M.A., Haug, G.H., Sarnthein, M., Tiedemann, R., Erlenkeuser, H., Stax, R.,
963 1995. Northwest Pacific Site 882: the initiation of Northern Hemisphere
964 glaciation. In: Rea, D.K., Basov, I.A., Scholl, D.W., Allan, J.F. (Eds.), Proc.
965 ODP, Sci. Res., 145, pp. 315–329.
- 966 Maslin, M.A., Li, X.S., Loutre, M.F., Berger, A., 1998. The contribution of orbital
967 forcing to the progressive intensification of Northern Hemisphere glaciation.
968 QSR 17, 411–426.
- 969 Mason, J.A., 2001. Transport direction of Peoria Loess in Nebraska and implications
970 for loess sources on the Central Great Plains. Quaternary Research 56, 79–86.
- 971 McGee, D., Broecker, W.S, Winckler, G., 2010. Gustiness: The driver of glacial
972 dustiness?, Quaternary Science Reviews 29 (17–18), 2340–2350,
973 doi:10.1016/j.quascirev.2010.06.009.
- 974 Millot, R., Allègre, C.J., Gaillardet, J., Roy, S., 2004. Lead isotopic systematics of
975 major river sediments: a new estimate of the Pb isotopic composition of the
976 Upper Continental Crust. Chemical Geology 203, 75–90.
- 977 Mix, A.C., Rugh, W., Pisias, N.G., Veirs, S., Leg 138 Shipboard Sedimentologists

North Atlantic Color Cycles

- 978 (Hagelberg, T., Hovan, S., Kemp, A., Leinen, M., Levitan, M., Ravelo, C), and
979 Leg 138 Scientific Party, 1992. Color reflectance spectroscopy: a tool for
980 rapid characterization of deep-sea sediments. *In* Mayer, L., Pisias, N., Janecek,
981 T, et al., Proc. ODP, Init. Repts., 138 (Pt. 1): College Station, TX (Ocean
982 Drilling Program), 67–77.
- 983 Mix, A.C., Harris, S.E., Janecek, T.R., 1995. Estimating lithology from nonintrusive
984 reflectance spectra: Leg 138. *In*: Pisias, N.G., Mayer, L.A., Janecek, T.R.,
985 Palmer-Julson, A., van Andel, T.H. (Eds.), Proc. of the Ocean Drill. Prog.,
986 Scientific Results, p. 138. 413–427.
- 987 Moulin, C., Lambert, C.E., Dulac, F., Dayan, U., 1997. Control of atmospheric export
988 of dust from North Africa by the North Atlantic oscillation. *Nature* 387, 691–
989 694.
- 990 Mudelsee, M., Raymo, M.E., 2005. Slow dynamics of the Northern Hemisphere
991 glaciation. *Paleoceanog.* 20, PA4022, doi:10.1029/2005PA001153.
- 992 Naafs, B.D.A., Stein, R., Hefter, J., Khélifi, N., De Schepper, S., Haug G.H., 2010.
993 Late Pliocene changes in the North Atlantic Current, *Earth Planet. Sci. Lett.*
994 298, 434–442, doi:10.1016/j.epsl.2010.08.023.
- 995 Naafs, B.D.A., Hefter, J., Acton, G., Haug, G.H., Martinez-Garcia, A., Pancost, R.,
996 Stein, R., 2012. Strengthening of North American dust sources during the late
997 Pliocene (2.7 Ma). *Earth Planet. Sci. Lett.* 317, 8–19.
- 998 Ortiz, J.D., Mix, A., Harris, S., O'Connell, S., 1999. Diffuse spectral reflectance as a
999 proxy for percent carbonate content in North Atlantic sediments. *Paleoceanog.*
1000 14, 171–186.
- 1001 O’Gorman, P., Schneider, T., 2009. Scaling of Precipitation Extremes over a Wide
1002 Range of Climates Simulated with an Idealized GCM. *Climate* 22, 5676–5685,

North Atlantic Color Cycles

- 1003 doi:10.1175/2009JCLI2701.1.
- 1004 Pausata, F.S.R., Li, C., Wettstein, J.J., Kageyama, M., Nisancioglu, K.H., 2011. The
1005 key role of topography in altering North Atlantic atmospheric circulation
1006 during the last glacial period. *Clim. Past* 7 (4), 1089–1101. doi:10.5194/cp-7-
1007 1089–2011.
- 1008 Prospero, J.M., Ginoux, P., Torres, O., Nicholson, S., Gill, T., 2002. Environmental
1009 characterization of global sources of atmospheric soil dust identified with the
1010 Nimbus 7 Total Ozone Mapping Spectrometer (TOMS) absorbing aerosol
1011 product. *Rev. Geophys.* 40(1), 1002, doi:10.1029/2000RG000095.
- 1012 Prentice, I.C., Harrison, S.P., Bartlein, P.J., 2011. Global vegetation and terrestrial
1013 carbon cycle changes after the last ice age. *New Phytologist* 189, ISSN:0028-
1014 646X, 988–998.
- 1015 Raymo, M.E., Ruddiman, W.F., Backman, J., Clement, B.M., Martinson, D.G., 1989.
1016 Late Pliocene variation in Northern Hemisphere ice sheets and North Atlantic
1017 deep water circulation. *Paleoceanog.* 4, 413–446.
- 1018 Raymo, M.E., Hodell, D.A., Jansen, E., 1992. Response of deep ocean circulation to
1019 initiation of northern hemisphere glaciation (3–2 Ma). *Paleoceanog.* 7, 645–
1020 672.
- 1021 Rea, D.K., 1994. The paleoclimatic record provided by eolian deposition in the
1022 deepsea: the geologic history of wind. *Reviews of Geophysics* 32 (2), 159–
1023 195.
- 1024 Raymo, M.E., Oppo, D.W., Flower, B.P., Hodell, D.A., McManus, J., Venz, K.,
1025 Kleiven, K.F., McIntyre K., 2004. Stability of North Atlantic water masses in
1026 face of pronounced climate variability during the Pleistocene. *Paleoceanog.*
1027 19, PA2008, doi:10.1029/2003PA000921.

North Atlantic Color Cycles

- 1028 Revel, M., Sinko, J.A., Grousset, F.E., Biscaye, P.E., 1996. Sr and Nd isotopes as
1029 tracers of North Atlantic lithic particles: paleoclimatic implications.
1030 *Paleoceanography* 11, 95–113.
- 1031 Ruddiman, W.F., Glover, L.K., 1972. Vertical Mixing of Ice-Rafted Volcanic Ash in
1032 North Atlantic Sediments. *Geological Society of America Bulletin* 83, 2817-
1033 2836.
- 1034 Ruddiman, W.F., McIntyre, A., 1976. "Northeast Atlantic Paleoclimatic Changes over
1035 the Past 600,000 Years. In *Investigation of Late Quaternary*
1036 *Paleoceanography and Paleoclimatology* edited by R.M. Cline and J.D.
1037 Hays, *Geol. Soc. of Am. Mem.* 145, 111–146.
- 1038 Ruddiman, W.F., 1977. Late Quaternary Deposition of Ice-Rafted Sand in Subpolar
1039 North-Atlantic (Lat 40-Degrees to 65-Degrees-N). *Geol. Soc. Am. Bull.* 8,
1040 1813–1827.
- 1041 Ruddiman, W.F., McIntyre, A., Raymo, M.E., 1987. Paleoenvironmental results from
1042 North Atlantic Sites 607 and 609. *Initial Reports DSDP* 94, 855–878.
- 1043 Ruddiman, W.F., Raymo, M.E., 1988. Northern hemisphere climate regimes during
1044 the past 3 Ma: Possible tectonic connections, in *The Past Three Million Years:*
1045 *Evolution of Climatic Variability in the North Atlantic Region*, eds. N.J.
1046 Shackleton, R. G. West, and D. Q. Bowen, p. 1-20, Cambridge University P
1047 ress, England.
- 1048 Ruddiman, W.F., Raymo, M.E., Martinson, D.G., Clement, B.M., Backman, J., 1989.
1049 Pleistocene Evolution: Northern Hemisphere Ice Sheets and North Atlantic
1050 Ocean. *Paleoceanog.* 4, 353–412.
- 1051 Salzmann, U., Haywood, A., Lunt, D.J, Valdes, P., Hill, D.J., 2008. A new global
1052 biome reconstruction and data-model comparison for the Middle Pliocene.

North Atlantic Color Cycles

- 1053 Global Ecology and Biogeography. 17(3). 432–447. ISSN 1466-822X.
- 1054 Salzmann, U. Haywood, A.M, Lunt., D.J. 2009. The past is a guide to the future?
- 1055 Comparing Middle Pliocene vegetation with predicted biome distributions for
- 1056 the twenty-first century. Phil. Trans. R. Soc. A 367, 189–204, doi:
- 1057 10.1098/rsta.2008.0200.
- 1058 Salzmann, U., Dolan, A.M., Haywood, A M., Chan W.-L., Hill, D.J., Abe-Ouchi, A.,
- 1059 Otto-Bliesner, B., Bragg, F., Chandler, M. A., Contoux, C., Dowsett, H.J., Jost,
- 1060 A., Kamae, Y., Lohmann, Lunt, D. J., Pickering, S.J., Pound M.J., Ramstein,
- 1061 G., Rosenbloom, N.A., Sohl, L., Stepanek, C., Ueda, H, Zhang, Z. (2013):
- 1062 Challenges in reconstructing terrestrial warming of the Pliocene revealed by
- 1063 data-model discord. Nature Climate Change.
- 1064 <http://dx.doi.org/10.1038/nclimate2008>.
- 1065 Seager, R., Ting, M., Held, I., Kushnir, Y., Lu, J., Vecchi, G., Huang, H.P., Harnik,
- 1066 N., Leetmaa, A., Lau, N.C., 2007. Model projections of an imminent transition
- 1067 to a more arid climate in southwestern North America. Science 316, 1181–
- 1068 1184, doi:10.1126/science.1139601.
- 1069 Seki, O., Foster, G.L., Schmidt, D.N., Mackensen, A., Kawamura, K., Pancost, R.D.,
- 1070 2010. Alkenone and boron-based Pliocene pCO₂ records. Earth Planet. Sci.
- 1071 Lett. 292, 201–211, doi:10.1016/j.epsl.2010.01.037.
- 1072 Seki, O., Schmidt, D.N., Schouten, S., Hopmans, E.C., Sinninghe Damsté, J.S.,
- 1073 Pancost, R.D., 2012. Paleoceanographic changes in the Eastern Equatorial
- 1074 Pacific over the last 10 Myr. Paleoceanography 27, PA3224,
- 1075 doi:10.1029/2011PA002158.
- 1076 Schefuß, E., Ratmeyer, V., Stuut, J.B.W., Jansen, J.H.F., Sinninghe Damste , J.S.,
- 1077 2003. Carbon isotope analyses of n-Alkanes in dust from the lower

North Atlantic Color Cycles

- 1078 atmosphere over the central eastern Atlantic. *Geochimica et Cosmochimica*
1079 *Acta* 67, 1757–1767.
- 1080 Shackleton, N.J., Backman, J., Zimmerman, H., Kent, D.V., Hall, M.A., Roberts,
1081 D.G., Schnitker, D., Baldauf, J.G., Desprairies, A., Homrighausen, R.,
1082 Huddlestun, P., Keene, J.B., Kaltenback, A.J., Krumsiek, K.A.O., Morton,
1083 A.C., Murray, J.W., Westberg-Smith, J., 1984. Oxygen isotope calibration of the
1084 onset of ice-rafting and history of glaciation in the North-Atlantic region.
1085 *Nature* 307, 620–623.
- 1086 Smith, G.A., 1994. Climatic influences on continental deposition during late-stage
1087 filling of an extensional basin, southeastern Arizona. *Geol. Soc. Am. Bull.*
1088 106, 1212–1228, doi:10.1130/0016-7606(1994)106<1212:CIOCDD2.3.CO>2.
- 1089 Stein, R., Hefter, J., Grutzner, J., Voelker, A., Naafs, B.D.A., 2009. Variability of
1090 surface water characteristics and Heinrich-like events in the Pleistocene mid
1091 latitude North Atlantic Ocean: Biomarker and XRD records from IODP Site
1092 1313 (MIS 16-9). *Paleoceanog.* 24, PA2203, doi:10.1029/2008PA001639.
- 1093 Steph, S., Tiedemann, R., Groeneveld, J., Sturm, A., Nürnberg, D., 2006. Pliocene
1094 changes in tropical East Pacific Upper Ocean stratification: response to
1095 tropical gateways? *Proc. Ocean Drilling Program Sci. Results* 202, 1–51.
- 1096 Sun, Y., An, Z., Clemens, S.C., Bloemendal, J., Vandenberghe, J., 2010. Seven
1097 million years of wind and precipitation variability on the Chinese Loess
1098 Plateau. *Earth and Planetary Science Letters* 297(3), 525–535.
- 1099 Tanaka, T., Togashi, S., Kamioka, H., Amakawa, H., Kagami, H., Hamamoto, T.,
1100 Yuhara, M., Orihashi, Y., Yoneda, S., Shimizu, H., Kunimaru, T., Takahashi,
1101 K., Yanagi, T., Nakano, T., Fujimaki, H., Shinjo, R., Asahara, Y., Tanimizu,
1102 M., Dragusanu, C., 2000. JNdi-1: a neodymium isotopic reference in

North Atlantic Color Cycles

- 1103 consistency with LaJolla neodymium. *Chemical Geology* 168 (3–4), 279–281,
1104 <http://dx.doi.org/10.1016/j.chemgeo.2007.03.021>.
- 1105 Taylor, S.R., McLennan, S.M., McCulloch, M.T., 1983. Geochemistry of loess,
1106 continental crustal composition and crustal model ages. *Geochimica et*
1107 *Cosmochimica Acta* 47, 1897–1905.
- 1108 Thierens, M., Pirlet, H., Colin, C., Latruwe, K., Vanhaecke, F., Lee, J.R., Stuut, J.-B.,
1109 Titschack, J., Huvenne, V.A.I., Dorschel, B., Wheeler, A.J., Henriët, J.-P.,
1110 2012. Ice-rafting from the British-Irish ice sheet since the earliest Pleistocene
1111 (2.6 million years ago): implications for long-term mid-latitude ice-sheet
1112 growth in the North Atlantic region. *Quaternary Science Reviews* 44, 229–
1113 230, doi:10.1016/j.quascirev.2010.12.020.
- 1114 Thompson, R.S., 1991. Pliocene environments and climates in the western U.S. *Quat.*
1115 *Sci. Rev.* 10, 115–132.
- 1116 Thompson, R.S., Anderson, K.H., 2000. Biomes of western North America at 18,000,
1117 6000 and 0 ¹⁴C yr BP reconstructed from pollen and packrat midden data. *J.*
1118 *Biogeogr.* 27, 555–584.
- 1119 Tiedemann, R., Sarnthein, M., Stein, R., 1989. Climatic changes in the western Sahara:
1120 Aeolo-marine sediment record of the last 8 million years (Sites 657–661).
1121 ODP, Sci. Results, 108: College Station, TX (Ocean Drilling Program), 241–
1122 277.
- 1123 Tiedemann, R., Sarnthein, M., Shackleton, N.J., 1994. Astronomic timescale for the
1124 Pliocene Atlantic $\delta^{18}\text{O}$ and dust flux records of Ocean Drilling Program Site
1125 659, *Paleoceanog.* 9, 619–638.
- 1126 Torrence, C., Compo, G.P., 1998. A practical guide to wavelet analysis, *Bull. Am.*
1127 *Meteorol. Soc.* 79, 61–78.

North Atlantic Color Cycles

- 1128 Ullman, D.J., LeGrande, A.N., Carlson, A.E., Anslow, F.S., Licciardi, J.M., 2014.
1129 Assessing the impact of Laurentide Ice Sheet topography on glacial climate.
1130 *Clim. Past* 10, 487–507, doi:10.5194/cp-10-487-2014.
- 1131 Vance, D., Thirlwall, M., 2002. An assessment of mass discrimination in MC-ICPMS
1132 using Nd isotopes. *Chemical Geology* 185 (3–4), 227–240,
1133 [http://dx.doi.org/10.1016/S0009-2541\(01\)00402-8](http://dx.doi.org/10.1016/S0009-2541(01)00402-8).
- 1134 Washington, R., Todd, M., Middleton, N.J., Goudie, A.S., 2003. Dust- storm
1135 source areas determined by the total ozone monitoring spectrometer and
1136 surface observations. *Ann. Assoc. Am. Geogr.* 93(2), 297–313.
- 1137 Watkins, S.J., Maher, B.A., Bigg, G.R., 2007. Ocean circulation at the Last
1138 Glacial Maximum: A combined modeling and magnetic proxy-based study.
1139 *Paleoceanography* 22, PA2204, doi:10.1029/2006PA001281.
- 1140 Werner, M., Tegen, I., Harrison, S.P., Kohfeld, K.E., Prentice, I.C., Balkanski, Y.,
1141 Rodhe, H., Roelandt, C., 2002. Seasonal and interannual variability of the
1142 mineral dust cycle under present and glacial climate conditions. *Journal of*
1143 *Geophysical Research* 107 (D24). doi:10.1029/2002JD002365
- 1144 Winkler, A., 1999. The climate history of the high northern latitudes since the middle
1145 Miocene: Indications from sedimentological and clay mineralogical analyses
1146 (ODP leg 151, central Fram strait), Reports on Polar Research, Alfred Wegener
1147 Institute for Polar and Marine Research, Bremerhaven, Germany, 344, 117 pp.
- 1148 Winkler, A., Wolf-Welling, T., Stattegger, K., & Thiede, J., 2002. Clay mineral
1149 sedimentation in high northern latitude deep-sea basins since the Middle
1150 Miocene (ODP Leg 151, NAAG). *International Journal of Earth Sciences*
1151 91(1), 133–148.
- 1152 Winckler, G., Anderson, R.F., Fleisher, M.Q., McGee, D. Mahowald, N., 2008.

North Atlantic Color Cycles

- 1153 Covariant glacial-interglacial dust fluxes in the Equatorial Pacific and
1154 Antarctica. *Science* 320, 93–96, doi: 10.1126/science.1150595.
- 1155 Wolfe J.A., Schorn H.E., Forest C.E., Molnar P., 1997. Paleobotanical evidence for
1156 high altitudes in Nevada during the Miocene, *Science* 276, 1672–1675,
1157 doi:10.1126/science.276.5319.1672.
- 1158 Zarate, M.A., Fasano, J.L., 1989. The Plio–Pleistocene record of the central eastern
1159 Pampas, Buenos Aires province, Argentina: the Chapadmalal case study.
1160 *Palaeogeogr., Palaeoclimatol., Palaeoecol.* 72, 27–52. doi:10.1016/0031-
1161 0182(89)90130-2.

1162

1163 **Figure captions**

1164 **Figure 1.** Lithostratigraphic cycles in North Atlantic deep-sea sediments of Plio-
1165 Pleistocene age in multiple drill sites as revealed by published physical property
1166 records. Sites arranged (from top to bottom) in order of increasing water depth. Note
1167 the existence of clear rhythmic cycles significantly earlier than MIS 100, the inferred
1168 glacial for the onset of basin-wide ice rafting. The data presented in the bottom panel
1169 (A) were originally compiled by Ruddiman et al. (1987, their Figure 3), although we
1170 substitute their record from DSDP Site 607 with our higher resolution proxy record
1171 from IODP Site U1313 (See Section 2.4 for methods). Those authors concluded that
1172 %CaCO₃ variability at pelagic DSDP Sites 607 (U1313) and 609, but not at the
1173 shallower DSDP Site 552, prior to Gauss/Matuyama boundary time was attributable
1174 to sea floor CaCO₃ dissolution, a consequence of the influence of corrosive poorly
1175 ventilated glacial intermediate waters in the North Atlantic. Top panel (B) shows data
1176 generated from additional shallow sites drilled after the Ruddiman et al., (1987) study
1177 (pelagic Site 982 (Shipboard Scientific Party, 1996), drift Site 980/981 (Ortiz et al.,

North Atlantic Color Cycles

1178 1999)). Note that the timing of the initiation of marked lithological cycles in the North
1179 Atlantic drill sites is not a simple function of water depth suggesting that CaCO_3
1180 dissolution is not the principle origin of these cycles (see text). The horizontal
1181 black/white bars in each panel denote paleomagnetic (sub)chronozone boundaries
1182 (Cande and Kent, 1995): B = Brunhes, M = Matuyama, G = Gauss, K = Keana, Ma =
1183 Mammoth and Gil = Gilbert.

1184

1185 **Figure 2.** North Atlantic region showing location of IODP Site U1313 relative to
1186 other drill sites referred to in the text (**A**) and mean April to September (the ‘dust
1187 season’; Prospero et al., 2002) surface wind vectors (**B**; image source
1188 <http://www.esrl.noaa.gov/psd/> (Kalnay et al., 1996)). Also shown in (**A**) is the last
1189 glacial maximum IRD-belt (stippled area) of Ruddiman (1977), relevant principal
1190 surface-ocean current systems (adapted from Kleiven et al., 2002) and average
1191 radiogenic isotope composition of potential source regions of terrigenous sediments
1192 deposited at Site U1313 (based on data shown in Figure 4).

1193

1194 **Figure 3.** Relationship between IODP Site U1313 sediment color (L^*) and calcium
1195 carbonate ($\%\text{CaCO}_3$) content. Global benthic oxygen isotope stack for the Plio-
1196 Pleistocene, the LR04 (Lisiecki and Raymo, 2005) and published benthic oxygen
1197 isotope data for IODP Site U1313 (**A**); discrete $\%\text{CaCO}_3$ measurements for late
1198 Pleistocene (**B**, black circles, Stein et al., (2009), $n = 151$) and late Pliocene and
1199 earliest Pleistocene (**C**, red circles, this study, $n = 193$) and our high resolution
1200 estimate of sediment $\%\text{CaCO}_3$ (against meters composite depth, mcd) based on least
1201 squares linear regression of L^* (5-point, 10 cm, moving average) onto discrete
1202 $\%\text{CaCO}_3$ measurements (**D**). Data corresponding to North Atlantic Hudson Strait
1203 Heinrich-like events (vertical grey bars in **B** labelled HE), for which the relationship

North Atlantic Color Cycles

1204 between L^* and $\%CaCO_3$ breaks down, are excluded from our least square regression.
1205 We identified Heinrich Layers at Site U1313 following Stein et al. (2009), based on
1206 their high (>500 cps) x-ray diffraction-derived dolomite concentrations. The
1207 horizontal black/white bars in each panel denote paleomagnetic (sub)chronozone
1208 boundaries (Cande and Kent, 1995): B = Brunhes, M = Matuyama, G = Gauss, K =
1209 Keana, Ma = Mammoth, Gil = Gilbert, C = Cochiti, N = Nunivak and S = Sidufjall.
1210 Depth range of chronozone boundaries shown in (B) and (C) based on shipboard
1211 measurements (Expedition 306 Scientists, 2006).

1212

1213 **Figure 4.** Characterisation of likely sources of terrigenous sediment to Site U1313 in
1214 Nd-Sr (A) and Pb-Pb (B & C) spaces. These fields are based on modern bedrock,
1215 loess, river sediment and aerosol data, and modern to LGM ice sheet/dust source
1216 proximal sediment core data. Potential sources constitute high-latitude material from
1217 Greenland and Northern Canada (the Canadian Province, Blue), volcanic material
1218 from Eastern Greenland and Iceland (Red, together with the Canadian Province this
1219 represents the most likely source of ice rafted material), mid-latitude material from
1220 Europe and the Gulf of St. Lawrence (purple) that is unlikely to be a significant
1221 source of ice-rafted material prior to significant northern hemisphere glaciation and
1222 potential aeolian sources from North America and the Sahara (green and yellow
1223 bubbles, respectively). Fields based on data from (also see Supplementary
1224 Information, Figures S1–S5): Abouchami and Zabel. (2003), Aleinkoff et al. (1999),
1225 Aleinkoff et al. (2008), Asmerom and Jakobsen (1993), Bernstein et al., (1998),
1226 Biscaye et al. (1997), Cohen and O’Nions (1982), Cole et al. (2009), Farmer et al.
1227 (2003), Goldstein and Jacobsen (1988), Grousset et al. (1988), Grousset et al. (2001),
1228 Hansen and Nielsen (1999), Juteau et al. (1986), Kokfelt et al. (1983), Kokfelt et al.

North Atlantic Color Cycles

1229 (2006), Millot et al. (2004), Revel et al. (1996).
1230
1231 **Figure 5.** Paleoceanographic records from IODP Site U1313 for the late Pliocene and
1232 earliest Pleistocene: **(A)** Foraminifera fragments as a percentage of total foraminifera
1233 plus fragments observed in the >150 μ m fraction (Ivanova et al., 2003). Overall, the
1234 carbonate material from this site is exceptionally well preserved. Modest increases in
1235 fragmentation are observed, however, during glacial periods from ca. 2.52 Ma
1236 onwards, demonstrating that more corrosive conditions existed at this site during
1237 glacials MIS 100, 98 and 96. For reference, we have included a line that approximates
1238 $\Delta(\text{CO}_3^{2-}) = 0$ in terms of percentage fragmentation based on Le and Shackleton
1239 (1992); **(B)** Benthic foraminiferal $\delta^{13}\text{C}$, measured on *Cibicidoides wuellerstorfi* (this
1240 study); **(C)** Alkenone mass accumulation rates, a productivity proxy (Naafs et al.,
1241 2010); **(D)** Mass accumulation rates, MAR, of n-alkanes and C26-alkan-1-ol, aeolian
1242 derived biomarkers (Naafs et al., 2012); **(E)** Calculated MAR of terrigenous material
1243 (this study); **(F)** Concentration of ice rafted coarse lithics (Ice rafted detritus, IRD,
1244 >150 μ m, excluding volcanics, which are only ever present in trace numbers).
1245 Transparent grey box shows the range of peak glacial values estimated for high-
1246 latitude North Atlantic Ocean DSDP Site 611 between MIS G6-100 (~2.72-2.5 Ma;
1247 Bailey et al., 2013). Overall, coarse lithic content of iNHG sediments at Site U1313 is
1248 extremely low (<50 grains g^{-1}) and prior to MIS 100 never higher than 5 grains g^{-1}
1249 (contrast with extremely high concentrations of 1500-5000 g^{-1} at Site 611); **(G)**
1250 Benthic $\delta^{18}\text{O}$ (Bolton et al., 2010) and L^* derived % CaCO_3 (this study), a remarkable
1251 correlation is seen. All data plotted on age model of Bolton et al. (2010). All MAR
1252 data shown estimated (as $\text{MAR} = \text{component abundance} \times \text{linear sedimentation rate} \times$
1253 dry bulk density) using sedimentation rates based on the age model of Bolton et al.

North Atlantic Color Cycles

(2010) and dry-bulk densities from shipboard determined GRAPE wet-bulk density data following the approach of Maslin et al. (1995). MARs shown in (C) and (D) recalculated on this basis using published datasets, but do not differ appreciably from original fluxes reported by Naafs et al. (2012). The horizontal black/white bars at the base of the figure denote paleomagnetic chronozone boundaries (Cande and Kent, 1995): M = Matuyama, G = Gauss, K = Keana and Ma = Mammoth.

Figure 6. Pb (A & B) and Nd-Sr (C) isotope composition of Plio-Pleistocene IODP Site U1313 bulk terrigenous sediments and range of radiogenic isotope values for potential terrigenous sources (as compiled in this study, see supplementary information, Figures S1–S5). Data from interglacial (triangles) and glacial (circles) samples are highlighted. Data uncertainty (at 2σ) is plotted, but usually smaller than symbols shown.

Figure 7. Time series of the radiogenic isotope composition of bulk terrigenous sediments deposited at IODP Site U1313: $^{87}\text{Sr}/^{86}\text{Sr}$ (A) ϵNd (B), $^{206}\text{Pb}/^{204}\text{Pb}$ (C). Benthic $\delta^{18}\text{O}$ stratigraphy for Site U1313 (Bolton et al., 2010) shown for reference. Grey dashed lines highlight relationship between data in (A-C) and glacial and interglacial marine isotope stages shown in (D). Data uncertainty (at 2σ) in A-C is smaller than symbols used. The radiogenic isotope composition of source regions shown on right hand side of figure (median – black line, 66th percentile – box, 95th percentile – “whisker”, outlying data-points marked as small crosses) are determined from data shown in Figure 4. Horizontal green lines denote the median of North American loess measurements, concluded to be the dominant source of Site U1313 terrigenous sediments (see main text). For comparison, Nd and Sr isotope

North Atlantic Color Cycles

1279 measurements from last glacial maximum ice rafting events at nearby drill cores
1280 (Sites SU90-08 and SU90-09 (Revel et al., 1996; Grousset et al., 2001)) are shown in
1281 (A) and (B). These data reveal extensive variability during the last glacial cycle (from
1282 -5.8 to -40.9 ϵNd , 0.72904 to 0.71662 $^{87}\text{Sr}/^{86}\text{Sr}$) and demonstrate that the radiogenic
1283 isotope systems studied are sensitive to large ice rafted debris inputs when present. Ice
1284 rafted debris is first observed at Site U1313 during MIS G6 (labelled in D). The
1285 horizontal black/white bars at the base of the figure denote paleomagnetic chronozone
1286 boundaries (Cande and Kent, 1995): M = Matuyama, G = Gauss, K = Keana and Ma
1287 = Mammoth.

1288
1289 **Figure 8.** Wavelet analysis of North Atlantic ODP Site 659 terrigenous accumulation
1290 rate (A) (Tiedemann et al., 1994), and Site U1313 terrigenous accumulation rate (B)
1291 and benthic oxygen isotopes (Bolton et al., 2010) (C). Wavelet spectra estimated
1292 following (Torrence and Compo, 1998). Solid black lines in each panel enclose
1293 regions of >95% confidence, based on a red-noise model (Torrence and Compo,
1294 1998). Within light shaded areas of panel B and C confident interpretation cannot be
1295 drawn due to edge effects (Torrence and Compo, 1998). These effects are not visible
1296 in (A) because we show only a central portion of a 5.3 Ma record analysed.
1297 Horizontal dashed grey lines on each panel labeled with 19, 23, 41 and 100 pick out
1298 dominant periodicities of orbital cycles. The dominant 20 ka, precessional cyclicity
1299 seen in Saharan dust inputs to Site 659 is not found in the mass accumulation rate of
1300 terrigenous sediment at Site U1313. The age model used for Site 659 is based on that
1301 published in Tiedemann et al. (1994). Re-analysis of the Site 659 terrigenous
1302 accumulation rate record following retuning of its benthic $\delta^{18}\text{O}$ stratigraphy to the
1303 LR04 stack (Lisiecki and Raymo, 2005) does not remove the strong 20 ka

North Atlantic Color Cycles

1304 precessional cyclicity shown in panel A (see Supplementary Information).

1305

1306 **Figure 9.** Cross plots of late Pliocene and earliest Pleistocene (3.33–2.41 Ma) IODP
1307 Site U1313 paleoceanographic and paleoclimate proxies: **(A)** Non-linear relationship
1308 between accumulation rates of terrigenous sediment (this study, interpreted as
1309 dominantly eolian dust) and dust-derived organic biomarkers (Naafs et al., 2012); **(B)**
1310 Non-linear relationship between global climate as recorded by benthic oxygen
1311 isotopes at Site U1313 (Bolton et al., 2010) and dust-derived organic biomarkers
1312 (Naafs et al., 2012); **(C)** Linear relationship between inferred eolian dust
1313 accumulation rates and dust-derived biomarker accumulation rates at Southern Ocean
1314 ODP Site 1090 (42°54.8'S, 8°54.0'E (Martinez-Garcia et al., 2011)). **(D)** Linear
1315 relationship between Site U1313 benthic oxygen isotopes (Bolton et al., 2010) and
1316 accumulation rates of terrigenous sediment (interpreted here as dominantly eolian
1317 dust). Note, we only plot data older than 2.41 Ma for Site U1313 when we can be
1318 confident that the bulk terrigenous sediment component at this site is dominated by
1319 eolian dust. Site 1090 data represent the last 4 Ma of aeolian dust deposition at this
1320 site. Biomarker accumulation rates used in this figure come from those plotted in
1321 Figure 4. Cross-plots in (A), (B) and (D) generated following linear interpolation of
1322 the terrigenous mass accumulation rate record to match the relatively lower resolution
1323 of the biomarker and benthic $\delta^{18}\text{O}$ data.

1324

1325 **Figure 10.** Time series of the ratio of accumulation rates of C26-alkan-1-ol and n-
1326 Alkane (Naafs et al., 2012) to terrigenous sediments at Site U1313. Both ratio time
1327 series are normalized to the average ratio observed for the Piacenzian PRISM time-
1328 slab (defined as 3.025–3.264 Ma). Biomarker accumulation rates used are the same as

North Atlantic Color Cycles

1329 those shown in Figure 5. Our higher-resolution record of terrigenous sediment
1330 accumulation rate is linearly interpolated to match the resolution of the biomarker
1331 records. The Site U1313 oxygen isotope stratigraphy (Bolton et al., 2010) is shown
1332 for reference, with key glacial marine isotope stages (M2, G6 and 100) labelled. Note,
1333 during glacial periods biomarker accumulation rates are enhanced relative to
1334 accumulation rates of bulk terrigenous material. The horizontal black/white bars at the
1335 base of the figure denote paleomagnetic chronozone boundaries (Cande and Kent,
1336 1995): M = Matuyama, G = Gauss, K = Keana and Ma = Mammoth.

1337

1338 **Figure 11.** The relationship between Site U1313 sediment lightness (L^*) and globally
1339 representative benthic $\delta^{18}\text{O}$, the LR04 (Lisiecki and Raymo, 2005) (A) and proxy
1340 indicators of the evolution of eastern equatorial Pacific (EEP) sea-surface temperature
1341 (B, based on alkenones from ODP Site 846 (Lawrence et al., 2006)) and sub-surface
1342 temperature (C, based on Mg/Ca ratios in foraminifer from ODP Sites 848, 849 and
1343 853 (Ford et al., 2012); ODP Site 1241 (Steph et al., 2006)). Horizontal dashed blue
1344 line in (B) corresponds to Holocene sea-surface temperature average for ODP Site
1345 846 (Lawrence et al., 2006). During the early Pliocene the mid latitudes of North
1346 America were wetter and warmer than present (Goldner et al, 2011). Note the warm
1347 temperatures of the EEP Ocean (associated with small zonal equatorial SST gradients
1348 (Ford et al., 2012), a state referred to as permanent El Niño-like (implies nothing
1349 about interannual variability). It is hypothesised that the development of the EEP cold
1350 tongue at this time and a subsequent poleward shift in the Pacific jet stream led to the
1351 aridification of North America (Goldner et al., 2011). Note that L^* at Site U1313, a
1352 proxy for sediment eolian content is unambiguously correlated to global climate
1353 (LR04) back to 3.3 Ma and intermittantly so probably back to 5.3 Ma (base of LR04),

North Atlantic Color Cycles

1354 the notable exception being ~4.3 to 4 Ma (see main text). For sediments older than 3.3
1355 Ma, our manual graphical correlation of Site U1313 and LR04 is based on tuning
1356 between constraints provided by shipboard determination of depths to
1357 paleomagnetostratigraphic boundaries (Expedition 306 Scientists, 2006). Age model
1358 control for ~2.4-3.3 Ma and <2.4 Ma, respectively, come from Bolton et al. (2010)
1359 and Naafs et al. (2012) and Expedition 306 Scientists (2006). The horizontal
1360 black/white bars at the top and base of the figure denote paleomagnetic chronozone
1361 boundaries (Cande and Kent, 1995): B = Brunhes, M = Matuyama, G = Gauss, K =
1362 Keana, Ma = Mammoth, Gil = Gilbert, C = Cochiti, N = Nunivak, S = Sidufjall and T
1363 = Thvera.

Figure 1

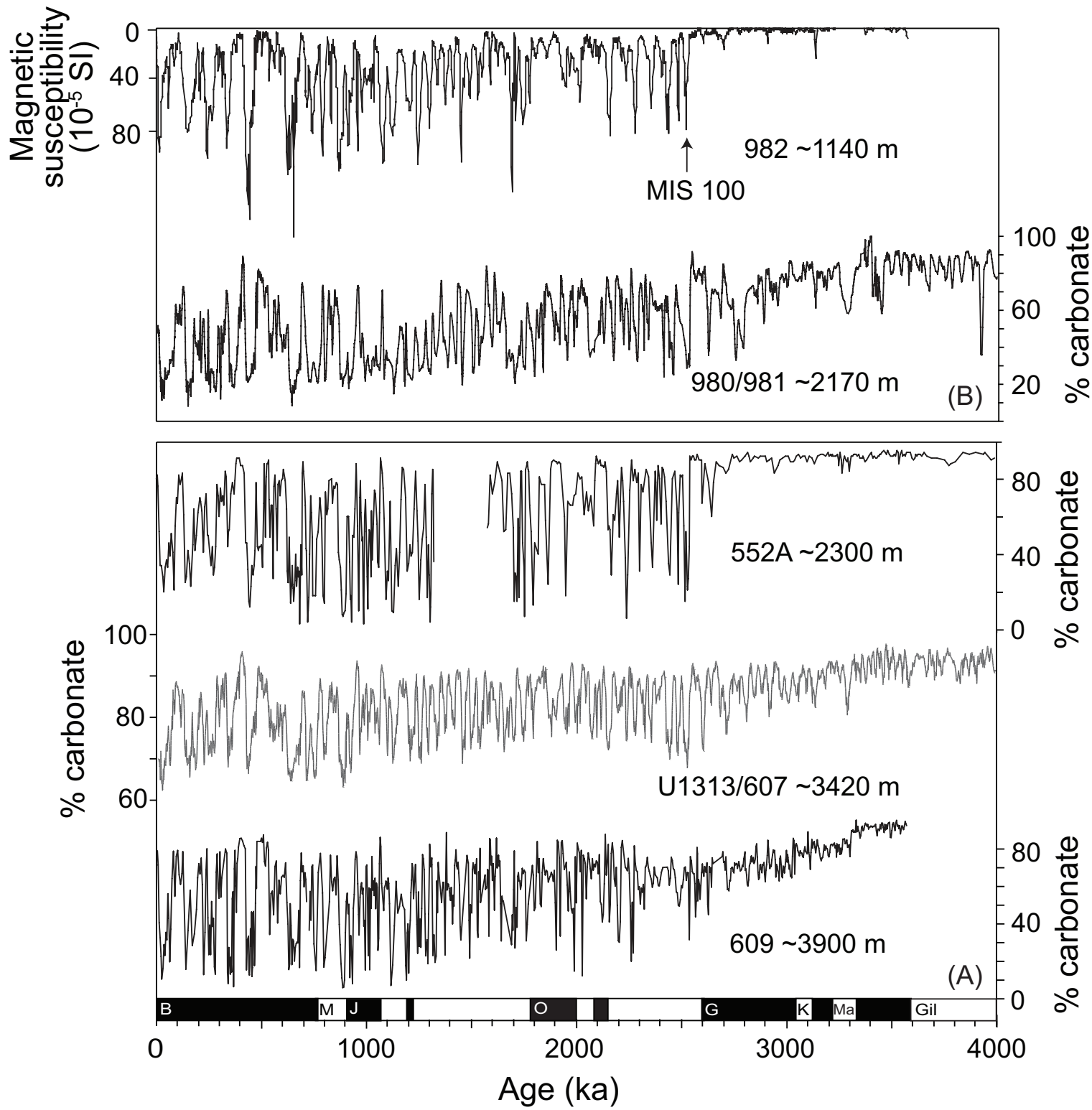


Figure 2

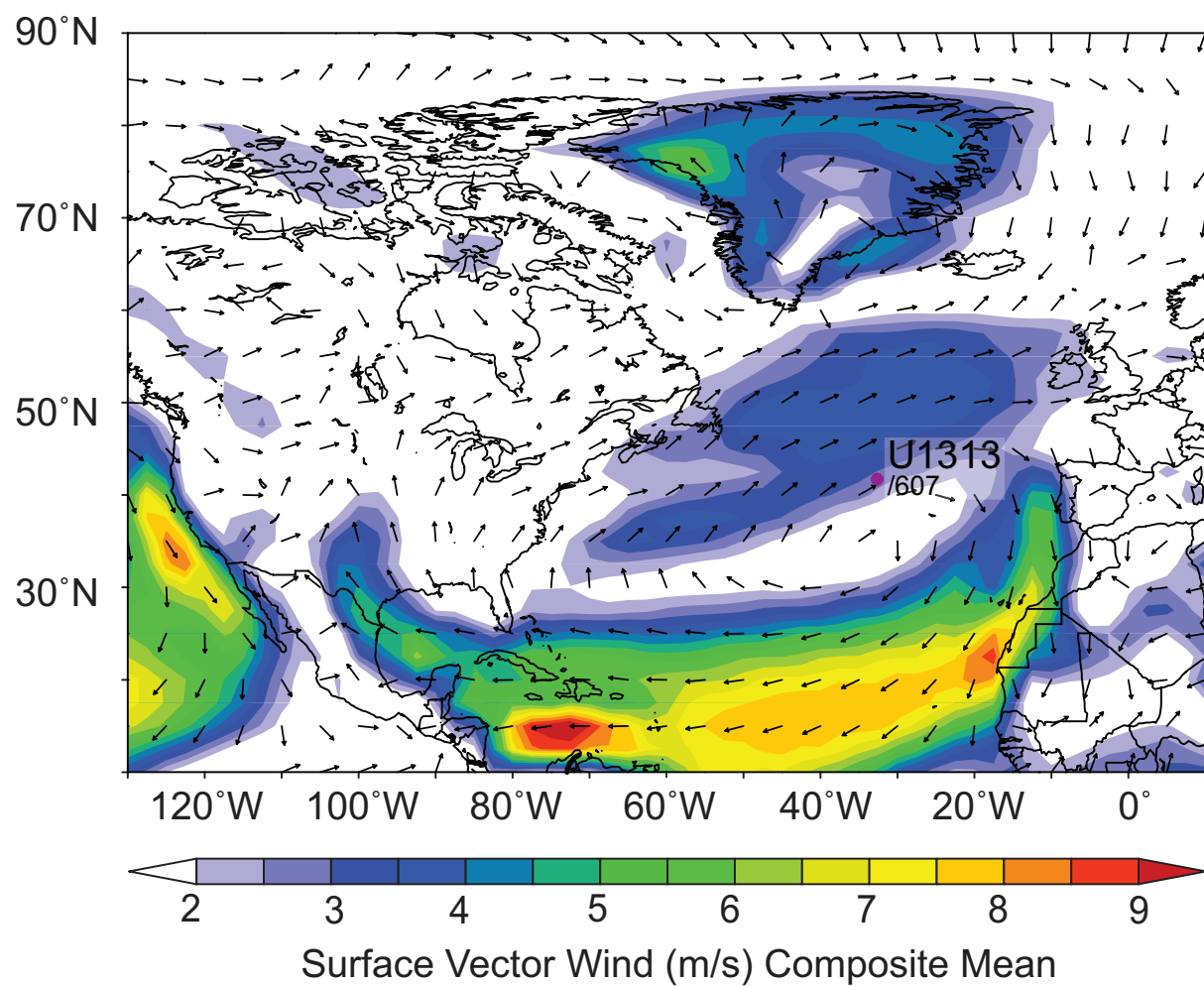
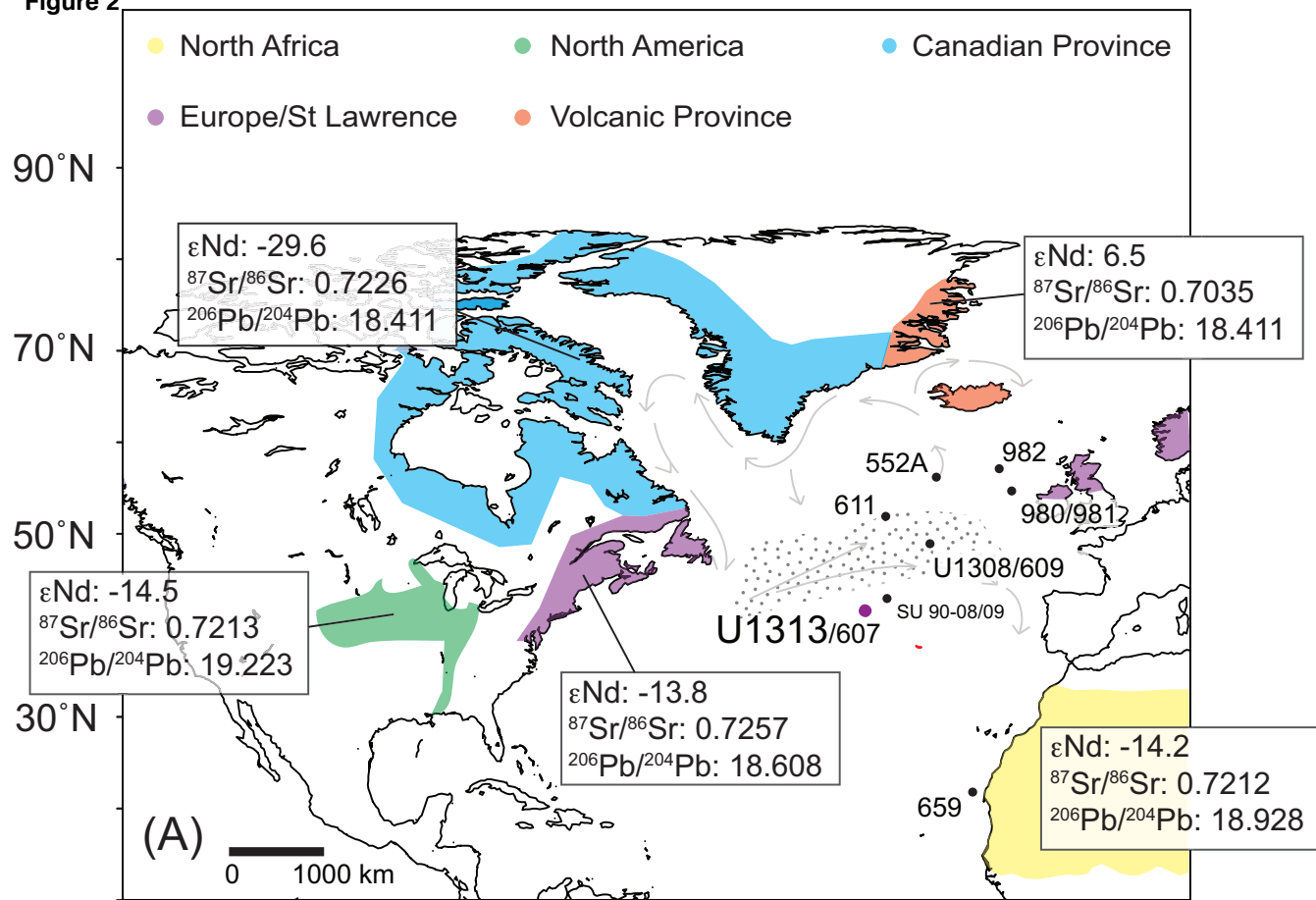


Figure 3

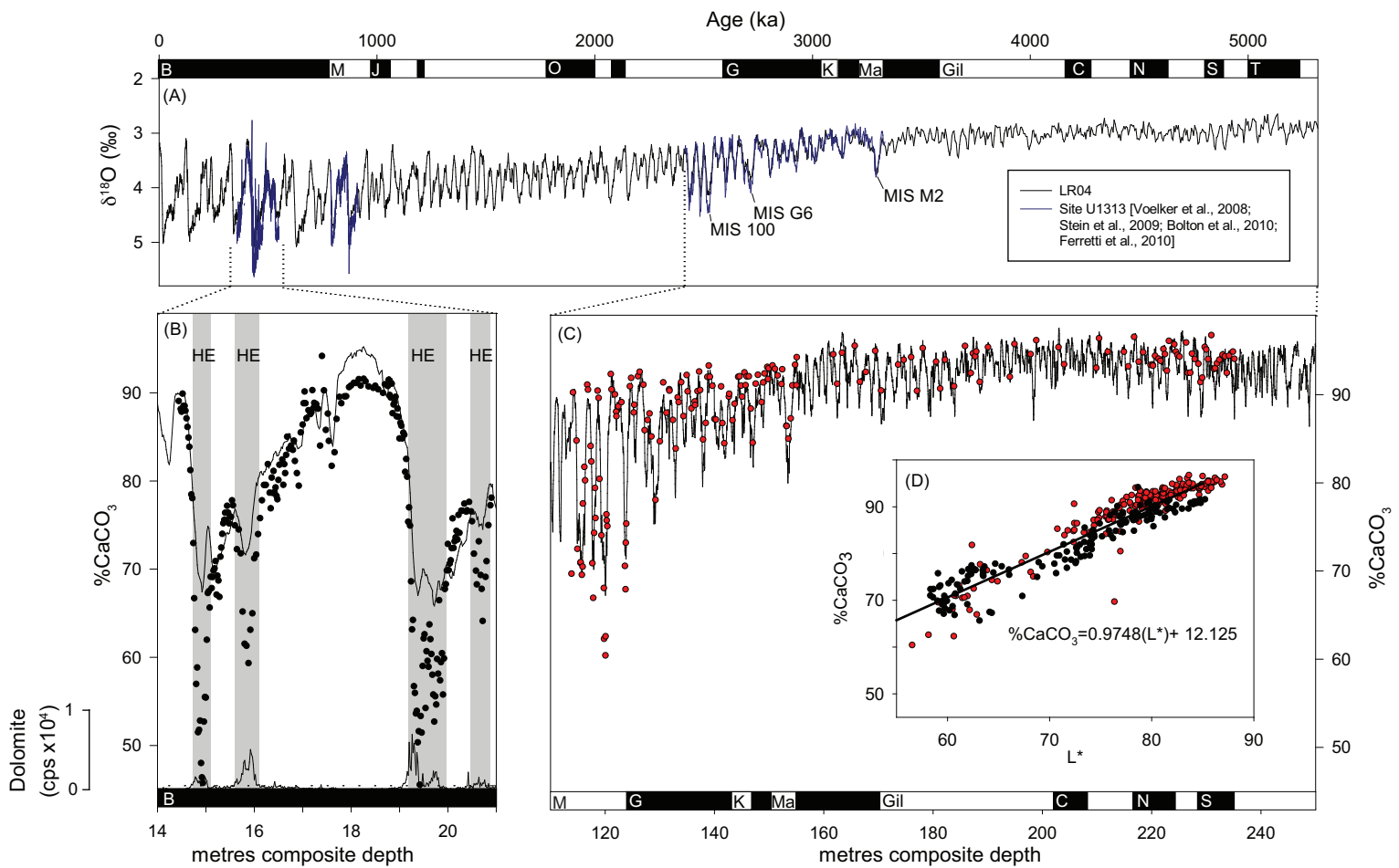


Figure 5

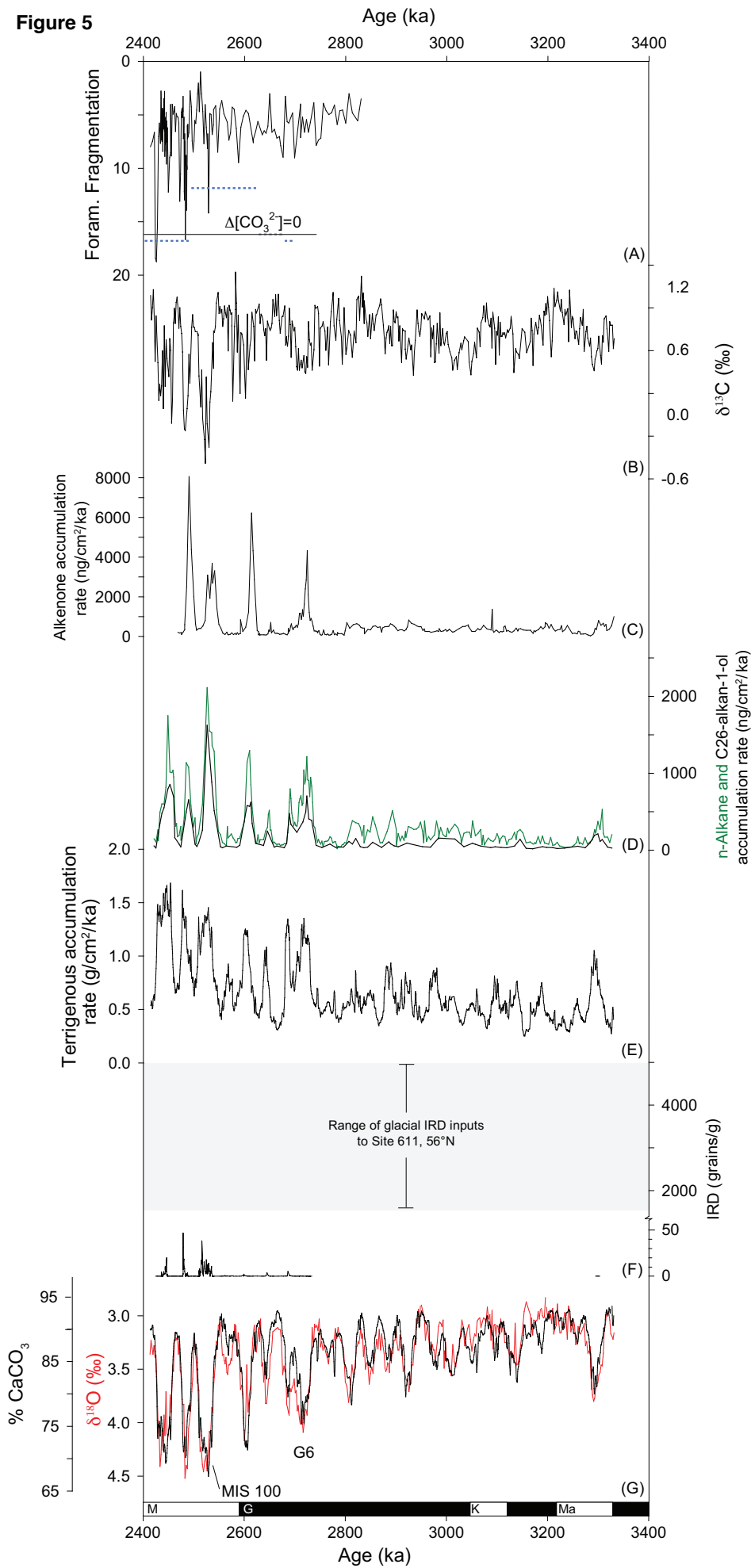


Figure 4

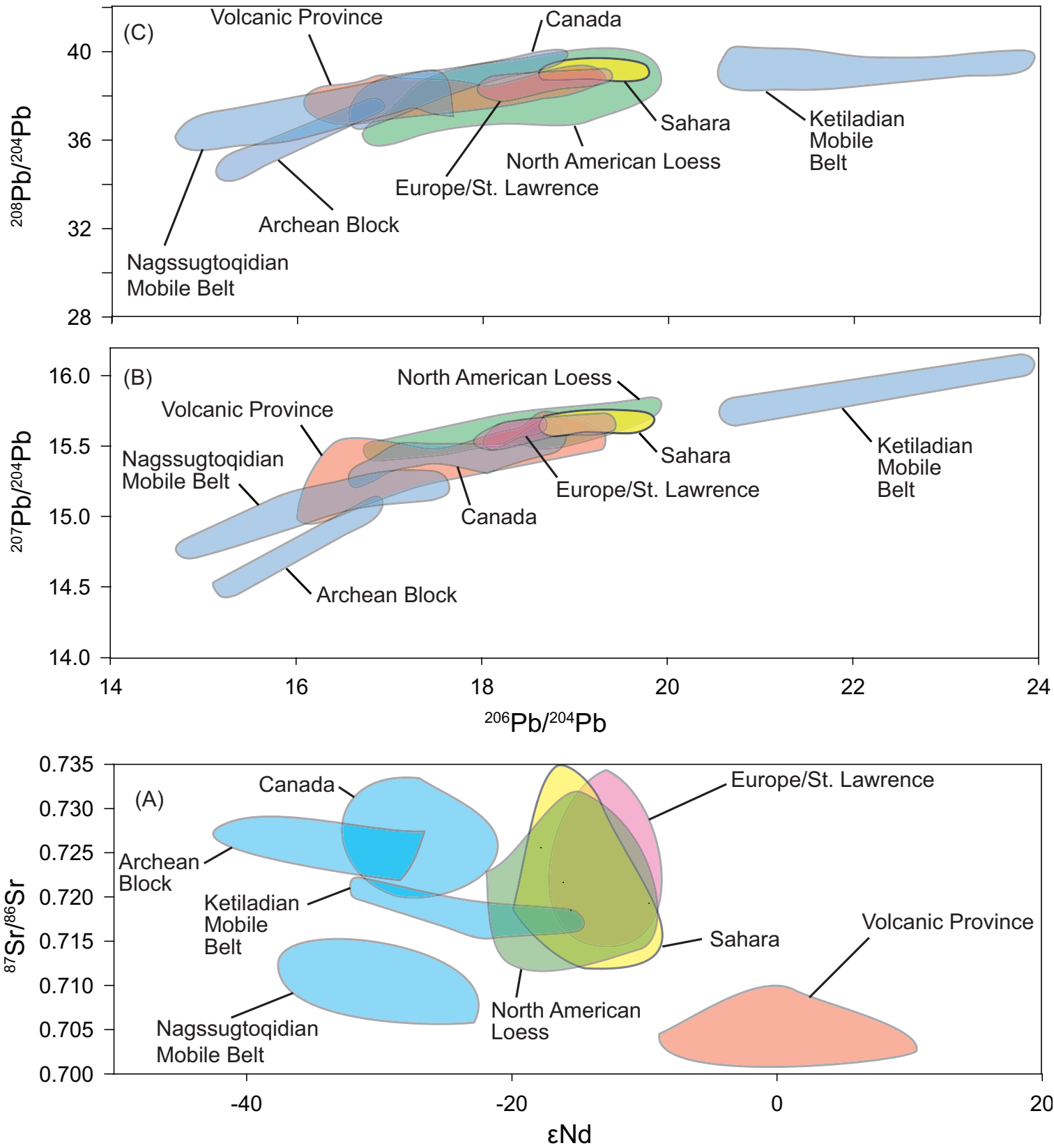


Figure 6

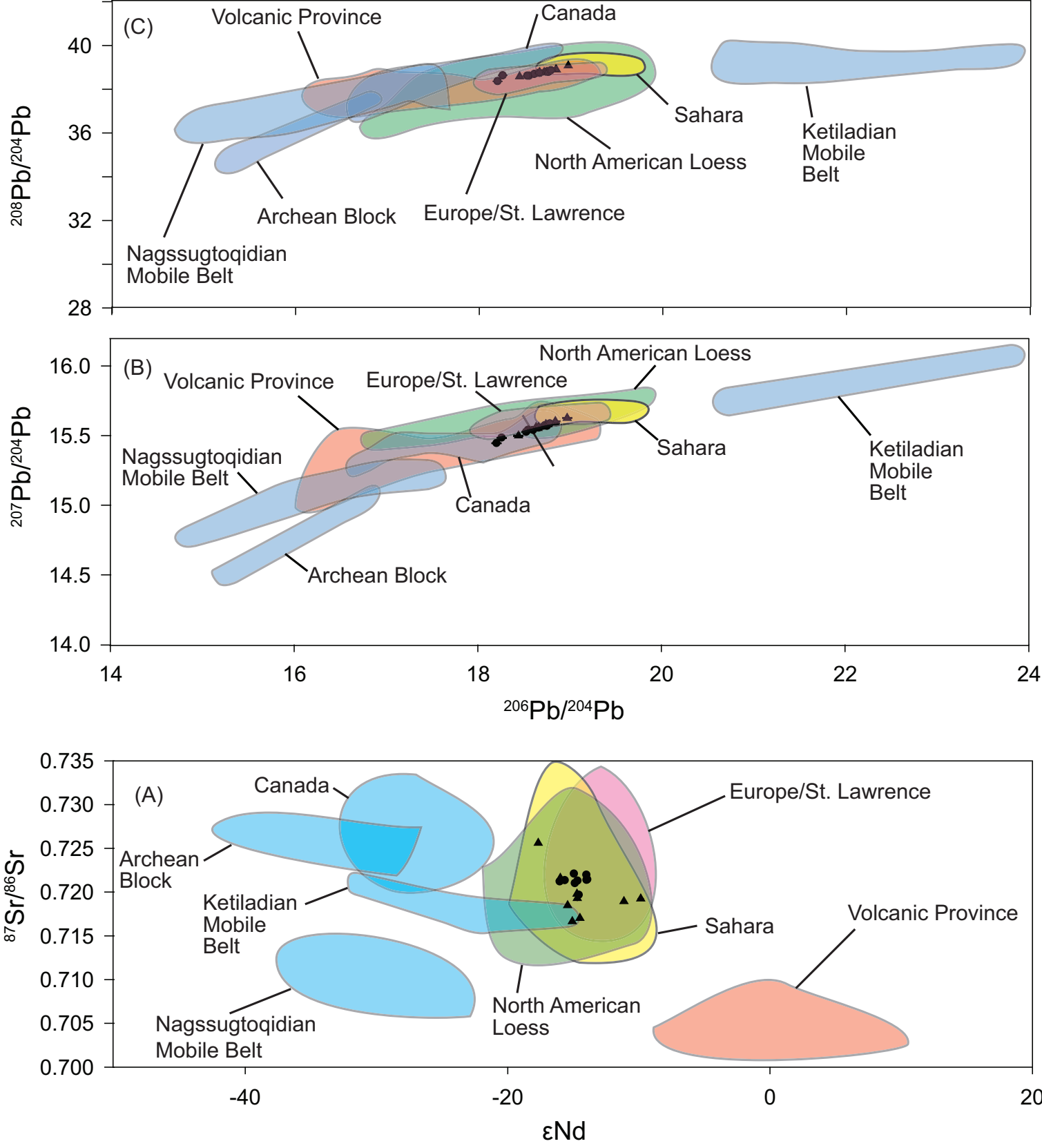


Figure 7

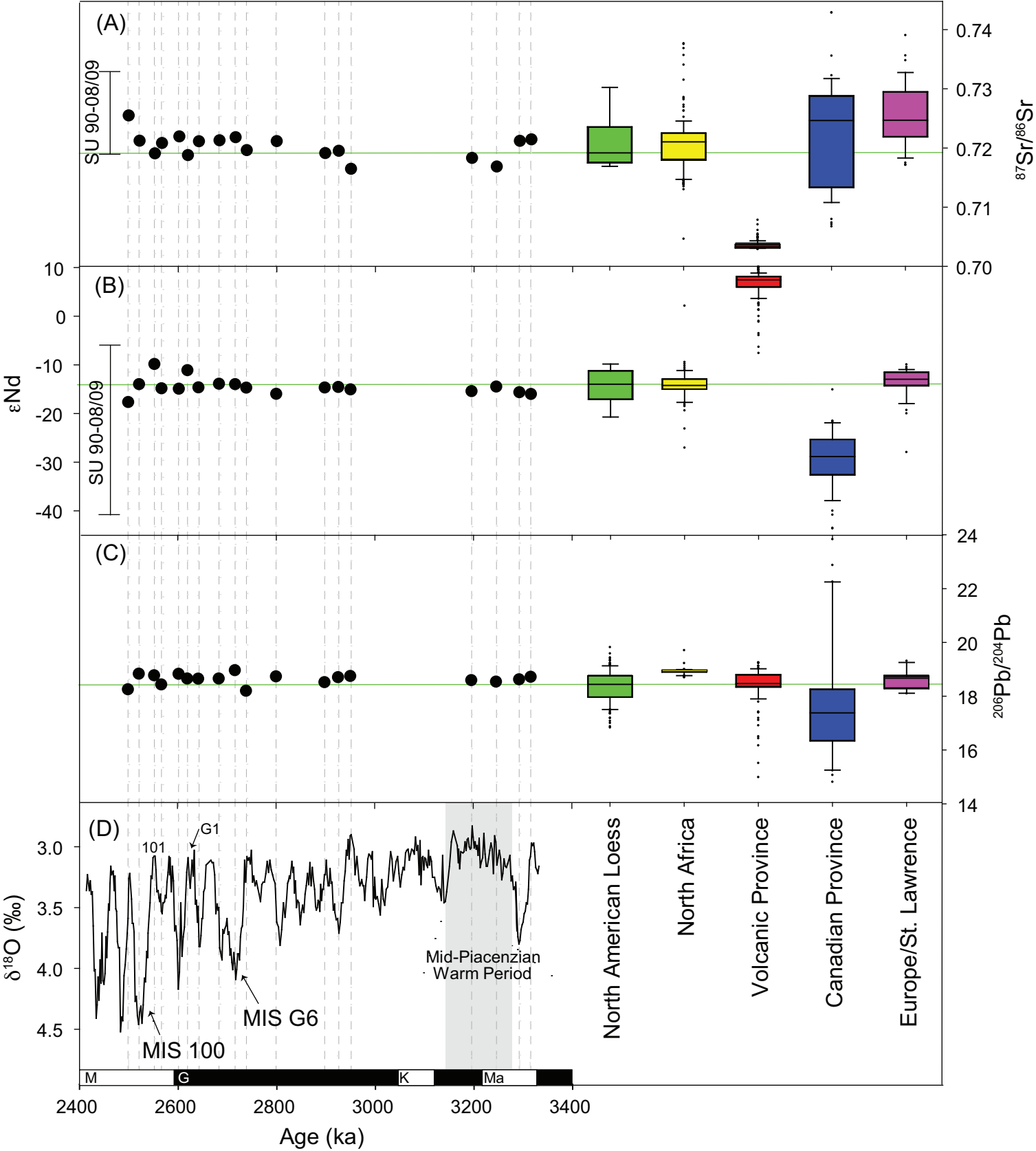


Figure 8

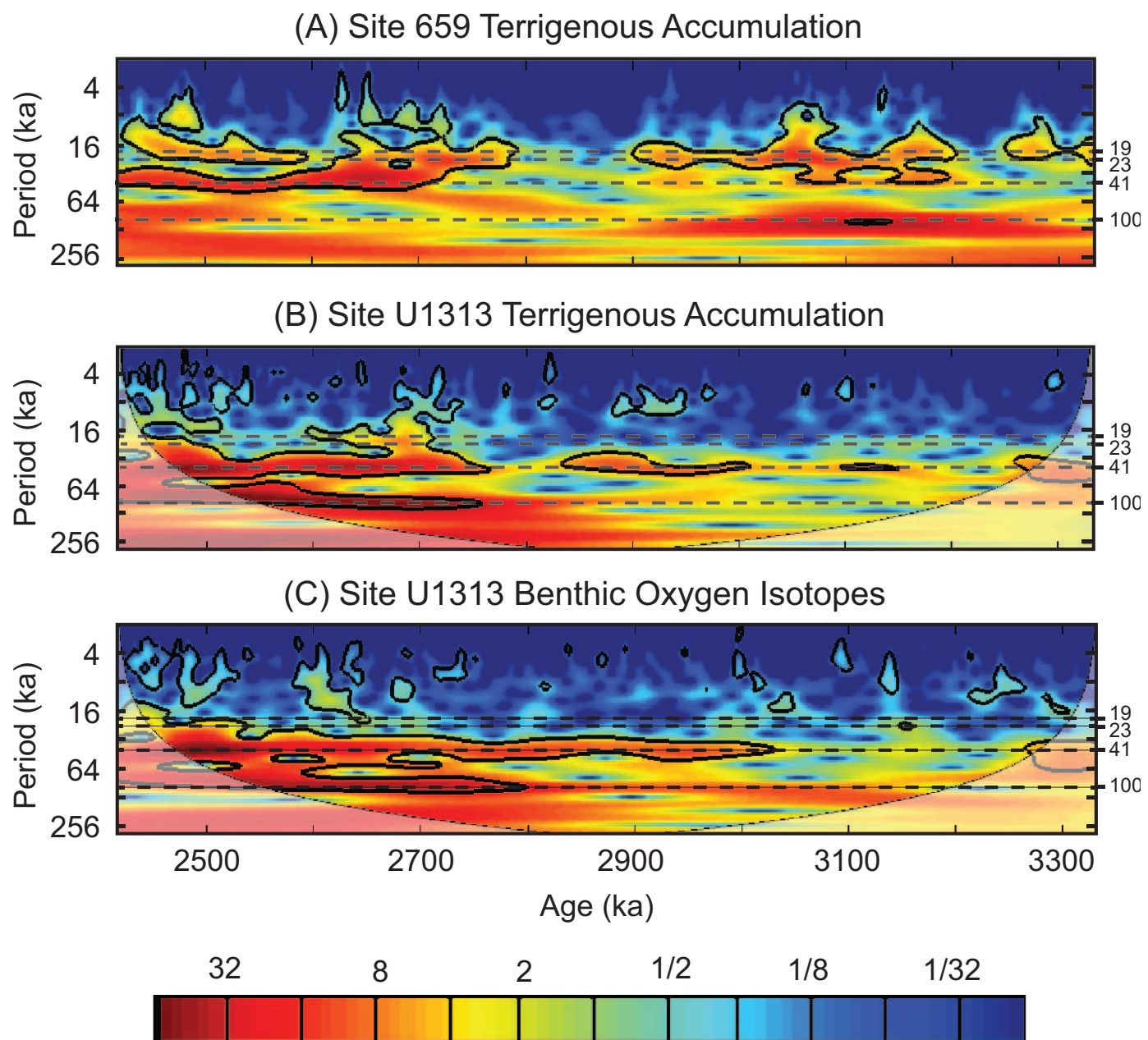


Figure 9

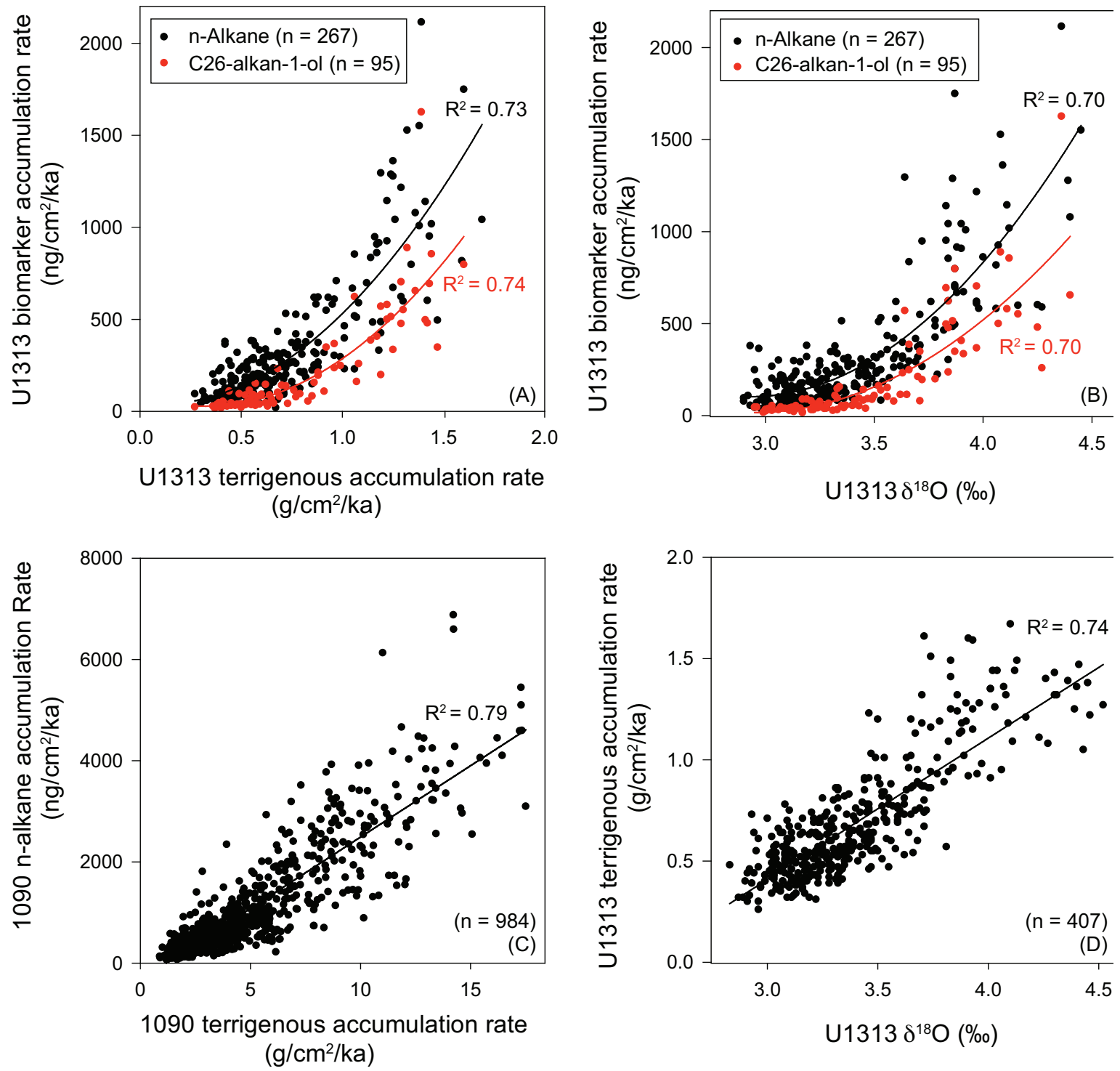


Figure 10

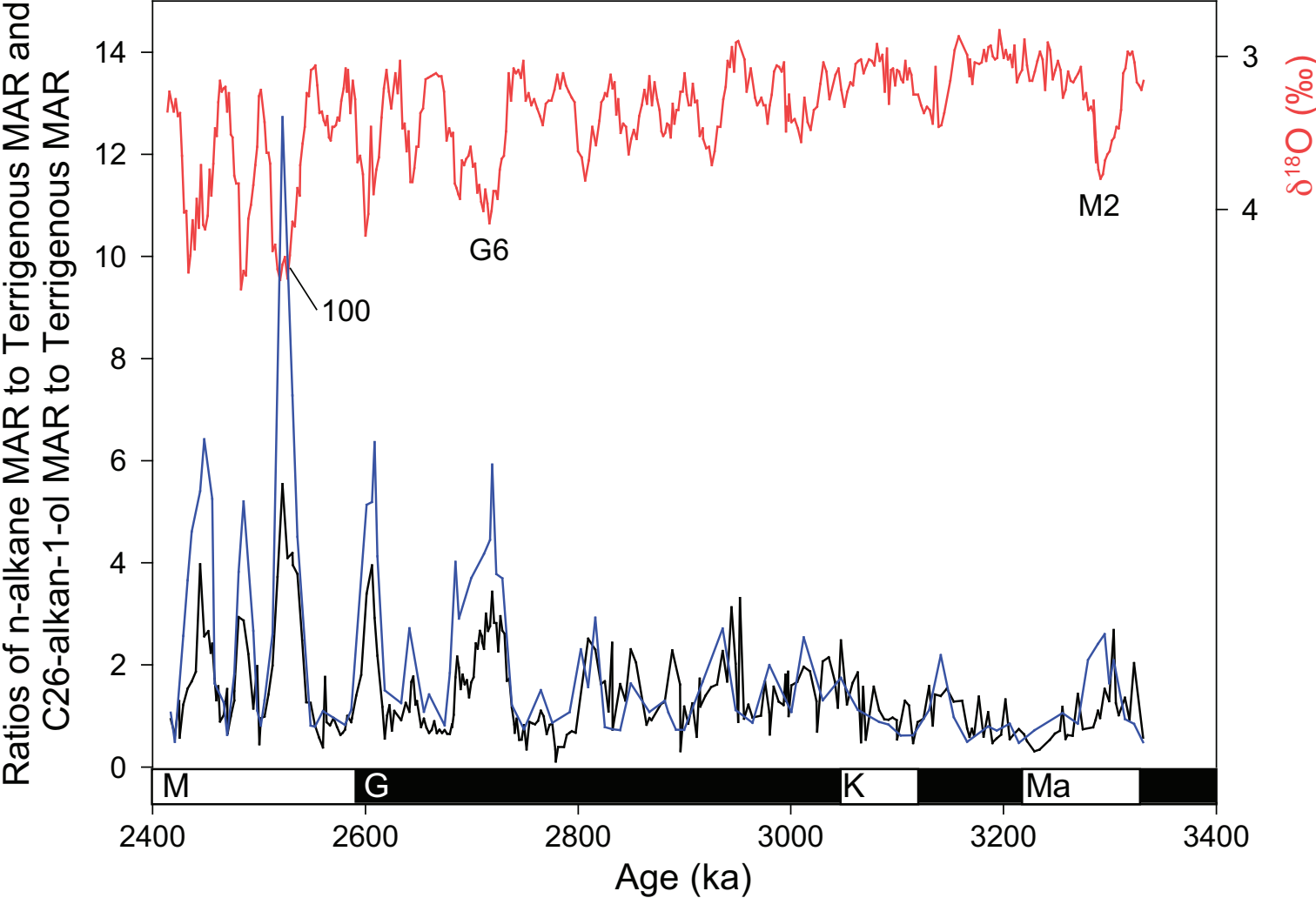
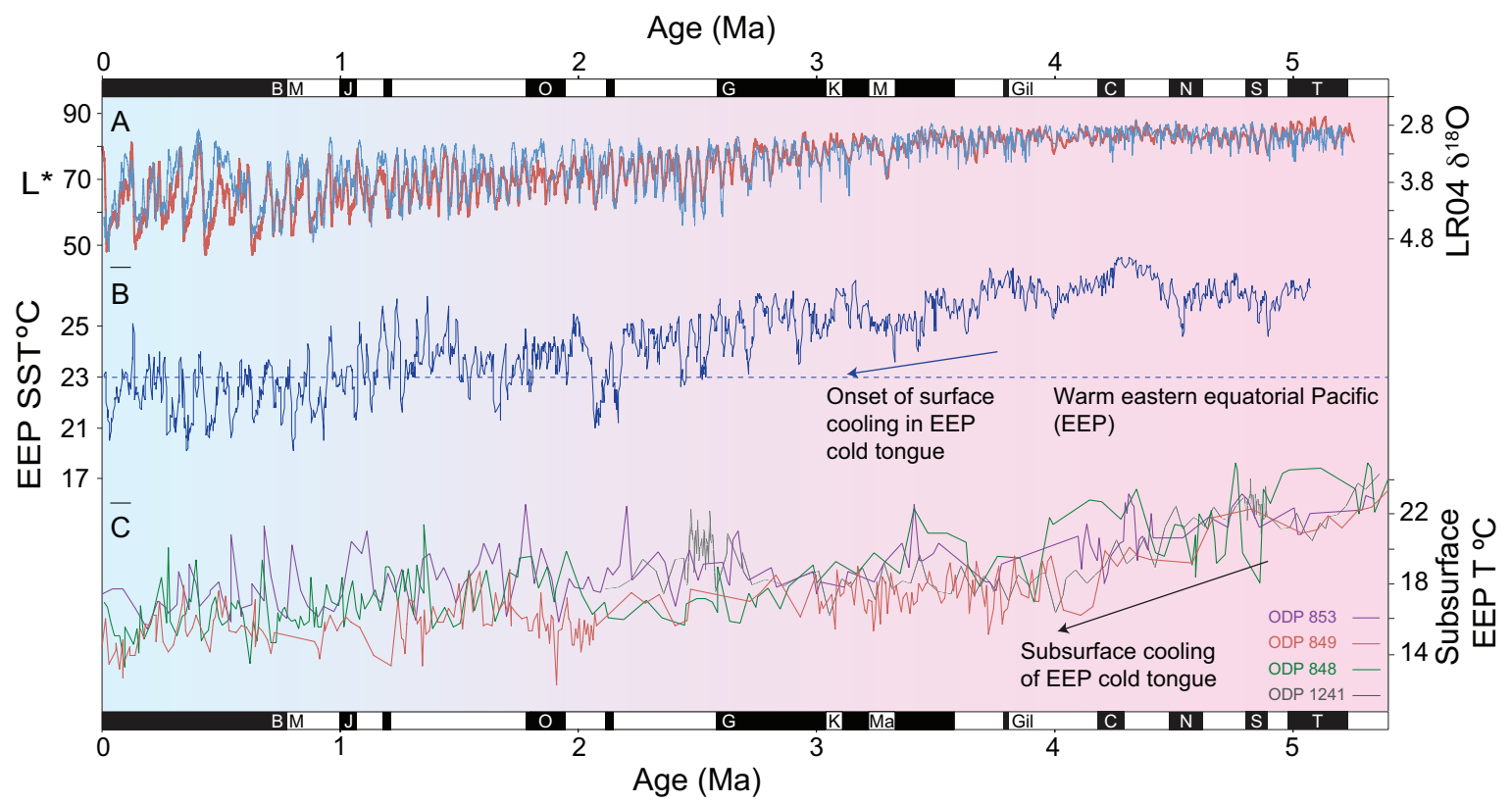


Figure 11



Supplementary Data

[Click here to download Supplementary Data: Lang et al. supplementary information.pdf](#)

'Equation File' for editorial office

[Click here to download Supplementary Data: Epsilon Nd equation.docx](#)